

AD A 0 47588

NORSAR

ROYAL NORWEGIAN COUNCIL FOR SCIENTIFIC AND INDUSTRIAL RESEARCH

12

Scientific Report No. 3-76/77

FINAL TECHNICAL SUMMARY

1 April - 30 September 1977

Edited by

H. Gjøystdal

DDC
RECEIVED
DEC 14 1977
F

Kjeller, 31 October 1977

Sponsored by
Advanced Research Projects Agency
ARPA Order No. 2551



AD No. —
DDC FILE COP

APPROVED FOR PUBLIC RELEASE, DISTRIBUTION UNLIMITED

REPORT DOCUMENTATION PAGE		READ INSTRUCTIONS BEFORE COMPLETING FORM
1. REPORT NUMBER F08606-77-C-0001	2. GOVT ACCESSION NO.	3. RECIPIENT'S CATALOG NUMBER
4. TITLE Norwegian Seismic Array (NORSAR).	5. TYPE OF REPORT & PERIOD COVERED 1 April 1977-30 September 1977	
7. AUTHOR(s) H. Gjølystdal (editor)	6. PERFORMING ORG. REPORT NUMBER Scientific Rep. 3-76/77	
9. PERFORMING ORGANIZATION NAME AND ADDRESS NTNF/NORSAR P.O. Box 51, N-2007 Kjeller, Norway	8. CONTRACT OR GRANT NUMBER(s) F08606-77-C-0001, ARPA Order-2551	
11. CONTROLLING OFFICE NAME AND ADDRESS Final Technical Summary	10. PROGRAM ELEMENT, PROJECT, TASK AREA & WORK UNIT NUMBERS NORSAR Phase 3	
14. MONITORING AGENCY NAME & ADDRESS (if different from Controlling Office) VELA Seismological Center 312 Montgomery Street Alexandria, Va. 22314 USA	12. REPORT DATE 31 October 1977	
16. DISTRIBUTION STATEMENT (of this Report) APPROVED FOR PUBLIC RELEASE; DISTRIBUTION UNLIMITED.	13. NUMBER OF PAGES 78	
17. DISTRIBUTION STATEMENT (of the abstract entered in Block 20, if different from Report) 31 Oct 77	15. SECURITY CLASS. (of this report) SECRET	
18. SUPPLEMENTARY NOTES NORSAR-SCIENTIC-3-76/77 NORSAR-CONTRIB-238	15a. DECLASSIFICATION/DOWNGRADING SCHEDULE	
19. KEY WORDS (Continue on reverse side if necessary and identify by block number)		
20. ABSTRACT (Continue on reverse side if necessary and identify by block number) <p>This report describes the operation and research activities at the Norwegian Seismic Array (NORSAR) for the period from 1 April to 30 September 1977.</p> <p>In this reporting period the NORSAR Online Detection Processor (DP) has been subject to a relatively low uptime percentage - only 88.8%, as compared to 95.5% for the previous period. The major contribution to</p>		

407283

the large downtime was a break in the Special Processing System (SPS) operation lasting for more than 17 days in July/August. This single event accounted for 84% of the total DP downtime, which was 490.5 hours. The operation of the Data Center has been taken care of by only 3-4 persons and this seems to work remarkably well, as the various users of the computer have now gained enough experience to run their own programs when working outside office hours. Due to the automatic telephone warning system triggered in case of DP breaks, one has been able to restart DP within 15-45 minutes in most cases. The performance of the data communication systems (including the ARPA network) can be characterized as good. There have been a few changes in the DP system, mainly connected with the ARPANET transmission mechanism and with the Online Event Processor. The regular operation of the old Event Processor system has been stopped, and a new program, AUTOEP, has been developed. This program, which will be run daily from 1 October 1977, prepares a complete detection list, an Event Bulletin and the corresponding Event Plots.

The array reduction work in the field was continued after the winter and completed within 1 October according to the original schedule. Approximately one half of the WHV/CTV's to be closed down were backfilled, whereas the other half were taken over by the landowners. Satisfactory performance and operation of the array instrumentation were maintained through this period in spite of the relatively high priority given to the array reduction work.

The research activities are documented in ¹⁰11 reports, which may be summarized as follows: The first report presents a study on interference of surface waves arriving simultaneously at the NORSAR array from more than one direction (1). Then follow four reports based on short period wave studies, one deals with travel time modelling using a continental array (2), one with theoretical amplitude calculations in comparison with NORSAR observations (3), one with upper mantle structure investigations using the Tau inversion method (4) and one with detection of waves converted from P to S in the mantle (5). The next report discusses bounds on long term noise variability (6), whereas the following one contains a work on short period discrimination using a multivariate autoregressive representation of P-waves (7). The last three reports are on statistical methods well suited for analyzing seismic data; the first one introduces a measure of association for spatial variables (8), the second one describes a criterion for determining the order of an autoregressive model (9), and the third one is a continuation of an earlier work on spectral estimation for spatial data (10).

H. Gjøystdal

AFTAC Project Authorization No. : VELA VT/7702/B/ETR
ARPA Order No. : 2551
Program Code No. : 7F10
Name of Contractor : Royal Norwegian Council for Scientific
and Industrial Research
Effective Date of Contract : 1 October 1976
Contract Expiration Date : 30 September 1977
Contract No. : F08606-77-C-0001
Project Manager : Nils Marås (02) 71 69 15
Title of Work : The Norwegian Seismic Array (NORSAR)
Phase 3
Amount of Contract : \$712.907
Contract Period Covered by the : 1 April - 30 September 1977
Report

The views and conclusions contained in this document are those of the authors and should not be interpreted as necessarily representing the official policies, either expressed or implied, of the Advanced Research Projects Agency, the Air Force Technical Applications Center, or the U.S. Government.

This research was supported by the Advanced Research Projects Agency of the Department of Defense and was monitored by AFTAC, Patrick AFB FL 32925, under contract no. F08606-77-C-0001.

NORSAR Contribution No. 238

ACCESSION for	
NTIS	Write Section <input checked="" type="checkbox"/>
DDC	Brief Section <input type="checkbox"/>
UNANNOUNCED	<input type="checkbox"/>
JUSTIFICATION	
BY	
DISTRIBUTION/AVAILABILITY CODES	
SPECIAL	
A	

TABLE OF CONTENTS

	<u>Page</u>
I. SUMMARY	1
II. OPERATION OF ALL SYSTEMS	3
II.1 Detection Processor (DP) Operation	3
II.2 Event Processor Operation	4
II.3 NORSAR Data Processing Center (NDPC) Operation	10
II.4 The ARPA Subnetwork (TIP to TIP, i.e., TIP incl. modems, lines and interfaces	12
III. IMPROVEMENTS AND MODIFICATIONS	15
III.1 Detection Processor	15
III.2 Event Processor	16
III.3 Array Instrumentation and Facilities	17
IV. MAINTENANCE ACTIVITY	19
V. DOCUMENTATION DEVELOPED	24
V.1 Reports, Papers	24
V.2 Program Documentation	24
VI. SUMMARY OF SPECIAL TECHNICAL REPORTS/PAPERS PREPARED	25
VI.1 Interference of Surface Waves	25
VI.2 P-wave Travel Time Studies using a Continental Array	30
VI.3 P-wave Amplitude Observations Across NORSAR - Observational and Theoretical Results	36
VI.4 Lateral P-velocity Distribution in the Upper Mantle Derived from NORSAR Data	49
VI.5 Detection of Waves Converted from P to SV in the Mantle	54
VI.6 Long Period Noise Level Variations at NORSAR	58
VI.7 Short-Period Discrimination Using Multivariate Autoregressive Representation of P-waves	62
VI.8 A Measure of Association for Spatial Variables	67
VI.9 A Criterion for Determining the Order of an AR Model	68
VI.10 A New Method of Spectral Estimation for Spatial Data. Part II.	70

I. SUMMARY

This report describes the operation and research activities at the Norwegian Seismic Array (NORSAR) for the period from 1 April to 30 September 1977.

In this reporting period the NORSAR Online Detection Processor (DP) has been subject to a relatively low uptime percentage - only 88.8%, as compared to 95.5% for the previous period. The major contribution to the large downtime was a break in the Special Processing System (SPS) operation lasting for more than 17 days in July/August. This single event accounted for 84% of the total DP downtime, which was 490.5 hours. The operation of the Data Center has been taken care of by only 3-4 persons and this seems to work remarkably well, as the various users of the computer have now gained enough experience to run their own programs when working outside office hours. Due to the automatic telephone warning system triggered in case of DP breaks, one has been able to restart DP within 15-45 minutes in most cases. The performance of the data communication systems (including the ARPA network) can be characterized as good. There have been a few changes in the DP system, mainly connected with the ARPANET transmission mechanism and with the Online Event Processor. The regular operation of the old Event Processor system has been stopped, and a new program, AUTOEP, has been developed. This program, which will be run daily from 1 October 1977, prepares a complete detection list, an Event Bulletin and the corresponding Event Plots.

The array reduction work in the field was continued after the winter and completed within 1 October according to the original schedule. Approximately one half of the WHV/CTV's to be closed down were backfilled, whereas the other half were taken over by the landowners. Satisfactory performance and operation of the array instrumentation were maintained through this period in spite of the relatively high priority given to the array reduction work.

The research activities are documented in 10 reports, which may be summarized as follows: The first report presents a study on interference of surface waves arriving simultaneously at the NORSAR array from more than one direction (1). Then follow four reports based on short period wave studies, one deals with travel time modelling using a continental array (2), one with theoretical amplitude calculations in comparison with NORSAR observations (3), one with upper mantle structure investigations using the Tau inversion method (4) and one with detection of waves converted from P to S in the mantle (5). The next report discusses bounds on long term noise variability (6), whereas the following one contains a work on short period discrimination using a multivariate autoregressive representation of P-waves (7). The last three reports are on statistical methods well suited for analyzing seismic data; the first one introduces a measure of association for spatial variables (8), the second one describes a criterion for determining the order of an autoregressive model (9), and the third one is a continuation of an earlier work on spectral estimation for spatial data (10).

H. Gjølystdal

II. OPERATION OF ALL SYSTEMS

II.1 Detection Processor (DP) Operation

There have been 107 breaks in the otherwise continuous operation of the NORSAR Online Detection Processor (DP) system within the reporting period. The uptime percentage is 88.8%, as compared to 95.5% for the last reporting period (October 1976 - March 1977).

Fig. II.1.1 and the accompanying Table II.1.1 both show the daily DP downtime in hours, for the days between 1 April and 30 September this year. The monthly recording times and up percentages are given in Table II.1.2.

As can readily be seen from Fig. II.1.1, the event with the most significant impact on the system operation is the SPS stop lasting for more than 17 days, starting on day 199. This is one of the longest stops in the history of the system. The interval length is directly related to the complexity of this subsystem and its poor hardware checkout facilities. Also, the IBM technicians' accumulation of knowledge on this machine, from one major stop to the next, seems to be insignificant.

The other major stops, lasting from 5 to 10 hours, are all caused by either the SPS going down or due to power failures.

The 107 breaks occurring within the reporting period may be grouped as follows:

a)	SPS malfunctioning	51
b)	Error on the multiplexor channel	15
c)	Stops related to program errors	14
d)	Stops related to program tests or changes	8
e)	Maintenance stops	6
f)	Power failures and jumps	4
g)	Magnetic tape drive problems	3

h)	Disk drive problems	2
i)	Other hardware problems	3
j)	Operational stops (system switch)	1

The SPS is thus causing the longest breaks and is also the most frequent cause of the system going down.

The error on the multiplexor channel is related to the volume of the traffic on this channel, occurring when the printer is used, or when the number of 1052 console typewriter messages is abnormally high (caused by some abnormal situation). However, the printer is used only for small intervals within the office hours and the 1052 stands idle during off-office hours. The durations of the infrequent stops caused by this error are therefore small.

During the first part of this period, a number of changes were made to the system, accompanied by 8 stops related to tests or initiations of new versions. Also, 14 stops more or less related to program errors occurred during the period. The number of stops in categories f) to h) are relatively normal.

The total downtime for this period was 490 hours 31 minutes. One SPS stop alone caused a downtime of 411 hours. The mean-time-between failures was 1.5 days as compared with 0.8 days for October 1976 - March 1977.

II.2 Event Processor Operation

The regular operation and maintenance of this system has been stopped. However, one-event processing may still be performed when starting parameters are entered via the 1052 Operator Console. The routine processing of results from the Online Event Processor is performed by the new AUTOEP program (see III.2).

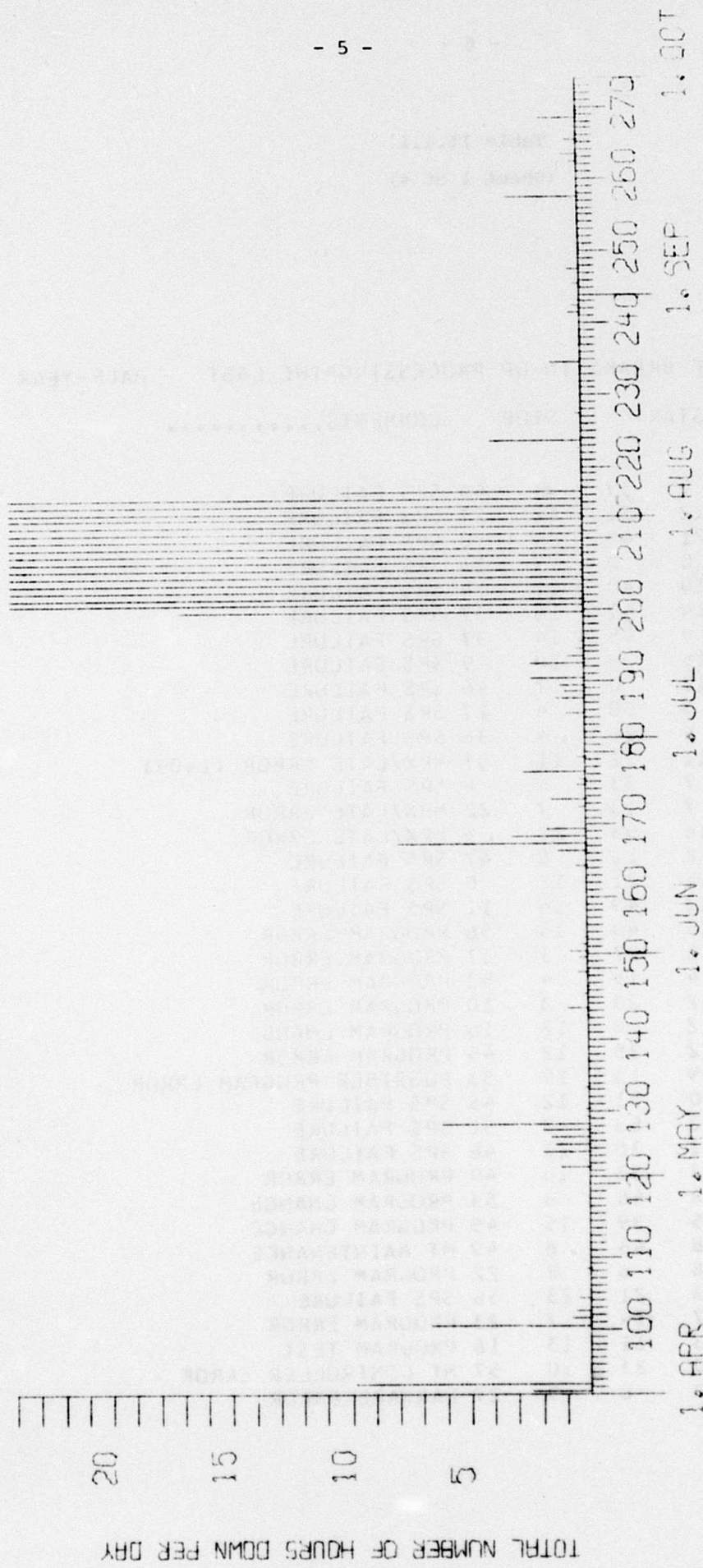


Fig. II.1.1.1 Detection Processor Downtime April - September 1977.

Table II.1.1
(Sheet 1 of 4)

LIST OF BREAKS IN DP PROCESSING THE LAST HALF-YEAR

DAY	START	STOP	COMMENTS.....
91	7	37	7 45 SPS FAILURE
91	12	21	12 27 SPS FAILURE
91	21	49	24 0 SPS FAILURE
92	0	0	7 23 SPS FAILURE
92	10	40	11 14 SPS FAILURE
92	14	47	16 37 SPS FAILURE
100	9	45	14 37 SPS FAILURE
100	15	9	16 9 SPS FAILURE
100	17	0	17 46 SPS FAILURE
101	3	50	4 17 SPS FAILURE
101	4	20	4 36 SPS FAILURE
102	11	22	11 57 MPX/LATE ERROR (1403)
104	7	33	8 4 SPS FAILURE
108	7	13	7 22 MPX/LATE ERROR
122	18	53	20 5 MPX/LATE ERROR
124	8	11	8 47 SPS FAILURE
124	11	21	12 0 SPS FAILURE
124	13	49	14 11 SPS FAILURE
124	15	40	15 56 PROGRAM ERROR
125	2	27	3 17 PROGRAM ERROR
125	4	18	4 52 PROGRAM ERROR
126	2	29	3 10 PROGRAM ERROR
126	12	8	12 16 PROGRAM CHANGE
126	12	35	12 45 PROGRAM ERROR
126	19	15	19 53 POSSIBLE PROGRAM ERROR
127	10	51	12 46 SPS FAILURE
128	2	53	8 51 SPS FAILURE
128	21	35	21 46 SPS FAILURE
129	13	33	13 40 PROGRAM ERROR
130	8	46	8 53 PROGRAM CHANGE
133	15	39	15 45 PROGRAM CHANGE
143	8	44	8 49 MT MAINTENANCE
144	8	6	8 22 PROGRAM ERROR
144	23	21	23 56 SPS FAILURE
146	7	14	7 23 PROGRAM ERROR
147	13	11	13 16 PROGRAM TEST
149	10	33	10 57 MT CONTROLLER ERROR
151	9	8	9 27 HARWARE ERROR

Table II.1.1 (cont.)

Sheet 2 of 4

LIST OF BREAKS IN DP PROCESSING THE LAST HALF-YEAR

DAY	START	STOP	COMMENTS,.....
152	8	13	8 34 PROGRAM CHANGE
152	12	29	12 49 PROGRAM ERROR
153	12	2	12 14 PROGRAM CHANGE
154	12	48	12 51 POSSIBLE PROG. ERROR
164	4	55	5 21 POWER JUMP
166	3	2	3 57 MT ERROR
166	13	30	13 44 MPX/LATE ERROR
167	1	26	7 37 POWER FAILURE
167	8	1	8 20 2841 TURNED ON
167	13	1	13 16 SPS FAILURE
167	21	50	22 56 SPS FAILURE
168	9	23	9 36 SPS FAILURE
168	19	2	21 55 SPS FAILURE
169	7	22	8 58 SPS FAILURE
172	12	8	12 20 MPX/LATE ERROR (1403)
173	9	58	10 9 SPS FAILURE
173	12	48	12 53 SPS FAILURE
173	13	44	13 52 SPS FAILURE
173	15	39	16 0 SPS FAILURE
173	17	21	18 2 SPS FAILURE
175	10	10	10 30 DISK DRIVE FAILURE
176	9	28	9 40 SPS FAILURE
177	19	8	21 43 DISK DRIVE FAILURE
179	9	38	9 56 CE MAINTENANCE
185	3	50	4 35 MPX/LATE ERROR
187	3	20	3 56 SPS FAILURE
187	13	50	14 24 MPX/LATE ERROR
188	11	9	11 40 MPX/LATE ERROR
188	13	21	13 38 SPS FAILURE
189	9	2	9 21 MPX/LATE ERROR
189	9	45	10 26 SPS FAILURE
190	7	26	8 26 SPS FAILURE
190	18	51	19 50 SPS FAILURE
190	19	54	20 9 SPS FAILURE
192	2	10	3 24 SPS FAILURE
192	5	24	5 46 SPS FAILURE
192	10	14	10 27 SPS FAILURE
192	19	13	19 36 SPS FAILURE

Table II.1.1 (cont.)

Sheet 3 of 4

LIST OF BREAKS IN OP PROCESSING THE LAST HALF-YEAR

DAY	START	STOP	COMMENTS.....
193	2	43	3 25 SPS FAILURE
194	6	54	7 MPX/LATE ERROR
195	13	52	14 0 MPX/LATE ERROR
199	7	5	24 0 SPS FAILURE/REPAIR
200	0	0	24 0 SPS FAILURE/REPAIR
201	0	0	24 0 SPS FAILURE/REPAIR
202	0	0	24 0 SPS FAILURE/REPAIR
203	0	0	24 0 SPS FAILURE/REPAIR
204	0	0	24 0 SPS FAILURE/REPAIR
205	0	0	24 0 SPS FAILURE/REPAIR
206	0	0	24 0 SPS FAILURE/REPAIR
207	0	0	24 0 SPS FAILURE/REPAIR
208	0	0	24 0 SPS FAILURE/REPAIR
209	0	0	24 0 SPS FAILURE/REPAIR
210	0	0	24 0 SPS FAILURE/REPAIR
211	0	0	24 0 SPS FAILURE/REPAIR
212	0	0	24 0 SPS FAILURE/REPAIR
213	0	0	24 0 SPS FAILURE/REPAIR
214	0	0	24 0 SPS FAILURE/REPAIR
215	0	0	24 0 SPS FAILURE/REPAIR
216	0	0	9 56 SPS FAILURE/REPAIR
216	13	21	13 30 SPS FAILURE/REPAIR
222	11	55	12 2 POSSIBLE PROG. ERROR
223	9	2	12 52 C E MAINTENANCE
227	7	13	7 25 MPX/LATE ERROR
234	10	20	10 59 MPX/LATE ERROR
234	15	3	15 37 MPX/LATE ERROR
241	6	10	6 18 HARDWARE ERROR
241	16	6	16 16 C E REPAIR
241	17	4	17 14 C E REPAIR
242	8	27	8 33 C E REPAIR
242	9	1	9 7 C E REPAIR
242	14	3	14 5 POSSIBLE PROGRAM ERROR
245	11	49	11 59 MT HARDWARE ERROR
245	13	30	13 33 PROGRAM CHANGE
247	3	6	3 36 SPS FAILURE
249	8	7	8 9 PROGRAM CHANGE
250	13	31	13 35 PROGRAM CHANGE

Table II.1.1 (cont.)

Sheet 4 of 4

LIST OF BREAKS IN DP PROCESSING THE LAST HALF-YEAR

DAY	START	STOP	COMMENTS.....
257	7	10	7 19 MPX/LATE ERROR
257	11	17	12 19 POWER FAILURE
257	16	12	18 1 POWER FAILURE
262	8	28	8 46 SPS FAILURE
263	10	26	10 31 SPS FAILURE
263	21	20	21 53 SPS FAILURE
265	12	50	13 7 SPS FAILURE
265	14	19	14 34 SPS FAILURE
268	14	33	15 22 SPS FAILURE, ONLINE TO B
268	23	15	24 0 SPS FAILURE
269	0	0	0 2 SPS FAILURE
272	7	45	7 50 ONLINE TO A

Table II.1.2
DP Computer Usage April - September 1977

Month	DP Uptime (hrs)	DP Uptime (%)	No. of DP Breaks	No. of Days with Breaks	DP MTBF* (days)
Apr	699.2	97.1	13	7	2.3
May	727.6	97.8	24	15	1.3
Jun	699.9	97.2	24	14	1.3
Jul	405.9	54.6	18	23	1.7
Aug	655.9	88.2	12	10	2.6
Sep	713.2	99.0	16	11	1.9
	3901.7	88.8	107	80	1.5

* Mean-time-between-failures.

II.3 NORSAR Data Processing Center (NDPC) Operation

Data Center

This period has been the first trial period for running the Data Center with just 3-4 persons, and so far this has been working remarkably well. The users of the job shop computer have gradually learned to operate so that they now run their own programs if they work outside office hours.

The Detection Processor uptime for the period is 88.8%. The reason for this low uptime is not the unmanned operation, but the bad performance of the SPS. The DP had about 30 stops outside office hours, most of them caused by the SPS. Except for a few stops before the alarm was properly fitted, the person on watch was called and was able to restart the DP after 15-45 minutes.

On 18 July the SPS stopped and was not running again until 4 August. Part of the reason for this long downtime is that this happened in the middle of the vacation with a resultant lack of qualified IBM personnel to work on it. Unfortunately, this failure - a bad card which was located and changed - does not seem to have anything to do with the failures that have caused the other stops as these have continued.

Maintenance of computer hardware was also in general taken care of by subcontractors during this period. Project personnel have intensified their engagement further compared to previous periods; this is especially true with respect to tape units and related equipment. By 1 October 1977 the Maintenance Agreement with IBM was reduced by nearly 50%. Individual machines withdrawn from the agreement will, if feasible, be maintained by project personnel, in difficult cases IBM will be called in to do maintenance service on time-spent and material-consumed basis.

Data Communication

Apart from sporadic and simultaneous outages of all circuits caused by carrier-frequency equipment, the performance in general must be characterized as very good. 43 outages occurred during the reporting period of which just a few had a duration of more than 1 hour.

Single subarrays communications systems have been affected by the usual reasons such as broken telephone cables, faulty equalizers, power failures, etc. Subarrays particularly affected are:

01A	Week 18/77	13% outage
	21/77	16.3% "
	22/77	6% "
	23/77	41.1% "
	24/77	29.4%
01B	Week 12/77	11.1% outage
	34/77	37.0% "
02C	Week 27/77	16.4% outage
	34/77	4.0% "
03C	Week 9/77	7.1% reduced performance (<200 errors per 16 2/3 min)
	11/77	8.6% "-
	28/77	13.2% outage
04C	Week 26/77	4.0% outage
	27/77	65.5% "
	28/77	8.9% "
06C	Week 9/77	7% reduced performance
	10/77	25.2% outage
	19/77	6.3% reduced performance.

As far as modems and related equipment are concerned, no observations indicate reduced reliability. One of the O1A modems (situated at NDPC) failed 8 August. The output level was low (-17.5 dB) and the separation filter (AHS-card) was replaced.

New equalizers/amplifiers are planned to be put into operation by NTA on all communications circuits weeks 43/44.

Table II.3.1 indicates outages/degraded performance pertinent to the different subarray communications circuits.

II.4 The ARPA Subnetwork (TIP to TIP, i.e., TIP incl. modems, lines and interfaces)

The London Communications Circuit

Apart from reduced line performance 13 April and loss of carrier 18 August, fair operation.

The SDAC Communication Circuit

Compared to previous periods satisfactory performance. Just minor irregularities observed. Loss of carrier occurred 13 April.

The Terminal Interface Message Processor (TIP) (Incl. modems and interfaces)
TIP preventive maintenance (PM) is carried out in accordance with BBN schedule.

From a hardware point of view the function of the TIP with accessories has been as expected. In two cases it has been necessary to replace parts: 1 TTY interface card (17 June) and 1 cooling fan (9 September). Modification to hardware was done 15 April when Bolt, Beranek and Newman (BBN) modified a Local Host Interface to become a Distant Host Interface for the Norwegian Defence Research Establishment (NDRE) 48 Kbit communications system. In the Teletype (TTY) a 60 Hz transformer was replaced with a 50 Hz transformer (1 June).

In the period 5 May to 1 June communication via the TTY (the IMPLINK facility) was impossible. Software was suspected at first, but a TTY interface card in the TIP caused the trouble.

It has also been difficult to run IMPLOAD in connection with special TIP program 'crashes'. First indication was 27 June when it failed a couple of times. 16 August a number of attempts were made before it was accepted. Last time, 8 September, it failed completely, and the paper tape stopped in the same position each time. This happened after the system power had been turned off during PM, when the CPU cooling fans (3) were found stopped due to a burned fan in the power unit, which had blown a common fuse. As no spare fan was available, it was disconnected and the fuse replaced. The Bootstrap Loader was reprogrammed manually in order to be able to get a program dump for a remote site in this way, but also that attempt failed.

Mr. C. Kelley of BBN arrived 9 September. Investigation revealed irregularities. After having 'cleaned the memory' and reprogrammed the 'Bootstrap' back to original, the IMPLOAD was accepted, and the system could resume operation again.

It is now, by means of a special cable, possible to bypass the TIP when it is down (for longer periods) and connect the London and SDAC modems together in order to maintain data exchange between the London TIP and the remaining network. Experiments done by S. Stowronski of BBN 19 September gave good results.

NDRE is now occupying 3 TIP interfaces:

1. A Very Distant Host I/F (SM-3/PDP-10)
2. A Distant Host I/F (Gateway, PDP-11)
3. A Modem I/F (9.6 Kbit codex modem)

Stage 2 of the Atlantic Satellite Experiment in which NDRE is engaged has involved movement of the 48 Kbit British Post Office (BPO) modem from NORSAR to NDRE, and rerouting of the 48 Kbit comm. line. The Gateway computer located at NDRE is now part of the new stage 2 configuration, and this machine is now via a private cable connected to the TIP.

The TIP has been restarted 15 times (excluding restarts during trouble shooting).

D. Rieber-Mohn, J. Torstveit, O.A. Hansen

Table II.3.1
Communications (degraded performance >20/outages >200). Figures in per cent of total time.
Month - 4 or 5 weeks as indicated (July 2, due to SPS outage)

Sub-array	Apr (4) (4.4-1.5) >20 >200	May (4) (2-29.5) >20 >200	June (5) (30.5-3.7) >20 >200	July (2) (4-17.7) >20 >200	Aug (5) (4.8-4.9) >20 >200	Spt (4) (5.9-2.10) >20 >200	Avg 1/2 year >20 >200
01A	1.2 1.5	1.5 29.3	1.1 84.0	0.7 1.8	1.1 0.9	1.8 3.2	1.2 20.1
01B	1.1 1.5	1.1 1.1	0.5 1.8	- 1.5	4.7 87.4	1.4 10.8	1.5 17.4
02B	1.0 0.2	0.2 0.5	0.4 1.3	- 1.6	1.7 0.7	1.8 2.8	0.9 1.1
02C	2.6 0.4	0.4 0.7	0.9 3.5	2.0 18.1	3.9 8.7	1.9 5.4	2.0 6.1
03C	1.4 1.0	0.8 0.5	1.0 1.8	0.4 14.1	1.2 3.1	1.8 2.9	1.1 3.9
04C	1.3 0.8	1.3 0.7	0.8 5.4	0.2 74.4	1.8 0.9	1.8 2.6	1.2 14.1
06C	0.2 0.7	7.4 0.7	0.8 4.1	- 1.5	1.5 0.9	1.8 2.4	2.0 1.7
AVG	1.3 0.9	1.8 4.8	0.8 14.6	0.5 16.1	2.3 14.7	1.8 4.3	1.4 9.2
Less		01A 0.7	01A 3.0	02C/03C/04C 1.6	01B 2.5	01B 3.2	01A/01B/04C 3.2

III. IMPROVEMENTS AND MODIFICATIONS

III.1 Detection Processor

The changes to this system have not been as many as for the last reporting period. However, some modifications have been implemented, mainly connected with the ARPANET transmission mechanism or with the Online Event Processor. As for the first type, the following changes were made:

- The ARPANET message builder (FNRSAD) will select and transmit (sections of) online or offline events, whenever available. Online events are always found in one of the 2 core buffers used for that purpose. Offline events will appear as queue entries in an internal queue, whenever the disk task has found anything to transmit in a certain disk file on the Shared Disk pack. Online events will always have priority over offline events during the selection process. However, once started, the transmission of any event will be completed before a new event is selected, regardless of its type.
- An automatic re-initialization of the ARPANET connection takes place after a certain time interval has elapsed. However, the length of this time interval has been made dependent on whether we have a 'Destination Dead' situation or not. If we have, 10 minutes will pass before re-initialization is performed, otherwise only 20 seconds is permitted after the last write operation before re-initialization is done.
- During a test period at the end of May, it was discovered that the total block length count in the VELANET message header and the block header in the incoming ARPANET messages had been changed from 148 to 150, according to a re-interpretation of the McCoy document. Since the bit pattern of these headers is used to verify the message in the NORSAR NCP task, all incoming messages had been discarded since early this month. After changing the verification pattern to be in accordance with the new conventions, incoming messages again were received without problems. Also, the corresponding changes were done to the outgoing ARPANET messages, including the length of the block header in the block length counts of the VELANET and block headers. The value of the count was thus increased to 212.

The following improvements and modifications were done to the Online Event Processor (PNREPX):

- Since it now and then happens that the start time for a coherent detection selected for event processing is zero (set too late), coding was inserted to construct the lacking start time by either using the start time for the corresponding incoherent detection, or, if none such was found, to use current time minus 10 seconds (DTINIT/2).
- The array beam delays, as extracted from the in-core tables during event processing, were stored in the Short Period Variable File (SPVF) section of the event output buffer (SPVF bytes 888-901).

In the beginning of June a software error that caused the system to go down infrequently was found and corrected. The Block Control Word (BCW) of the first queue block in Queue storage was overwritten by any Location Parameter Table segment loaded into core. The system then went down if it tried to re-use the queue block with the destroyed BCW. The error was corrected by loading Queue Storage as a separate phase.

III.2 Event Processor

In order to obtain the results from the Online Event Processor (OEP), which are written to the Detection Log Tape, a new offline program, AUTOEP, has been developed. This program, which will be run daily, reads all Detection Log tapes to extract the OEP result records found there, and presents these results in the form of

- a complete Detection List
- an Event Bulletin (list and punched cards), and
- Event Plots.

There are algorithms for event arrival time refinement and for the extraction of an event's dominant period and amplitude embedded in this program. A filtered array beam is used for this purpose, and the results are afterwards compensated for filter and system response. The Event Plot (see Fig. III.2.1) consists of 3 representations of the Array Beam (scaled to the noise level and clipped, scaled to the signal level, and filtered), 7 subarray beams and one single sensor. Markers ('tics') for every minute

half minute and 10 seconds intervals are superimposed upon the traces. Complete documentation of this program is presently being written and will appear later. However, changes/improvements in this system are likely to occur for some time yet.

D. Rieber-Mohn

III.3 Array Instrumentation and Facilities

The array reduction work was resumed in May after dryup of the array access roads after winter. The schedule was kept, thus within 1 October all this work was completed. In addition to administrative and store room work, 123 days' work were spent in the field exclusively for the array reduction activity. Of the 80 WHVs to be closed down (including 60 m deep holes in the B-ring) 42 were backfilled with nearby available filling material, 32 were given to the landowners for their use and responsibility, and one (04B05) was excepted from the close down, as this WHV is used for the NORSAR Analog Station. Three CTV/LPVs (01C, 08C and 11C) were completely sealed with concrete including backfilling; the twelve others were taken over by the landowners. All equipment except for a few items (i.e., the steel drums in the WHVs, some of the inventory in the CTVs) were brought to NMC where it is grouped and stored in the main storage.

A.K. Nilsen

BP-8 1-4-3-4 42

EPX 21850

27 OCT 1977 (DDY 300)

NCRSAR BULLETIN

2 0 22 35 31.0N 50.0E 330 D +4.5 346 IRAN
3 0 30 0.8 NB2 # 10.1 0.6 12.2 39.4 115.4

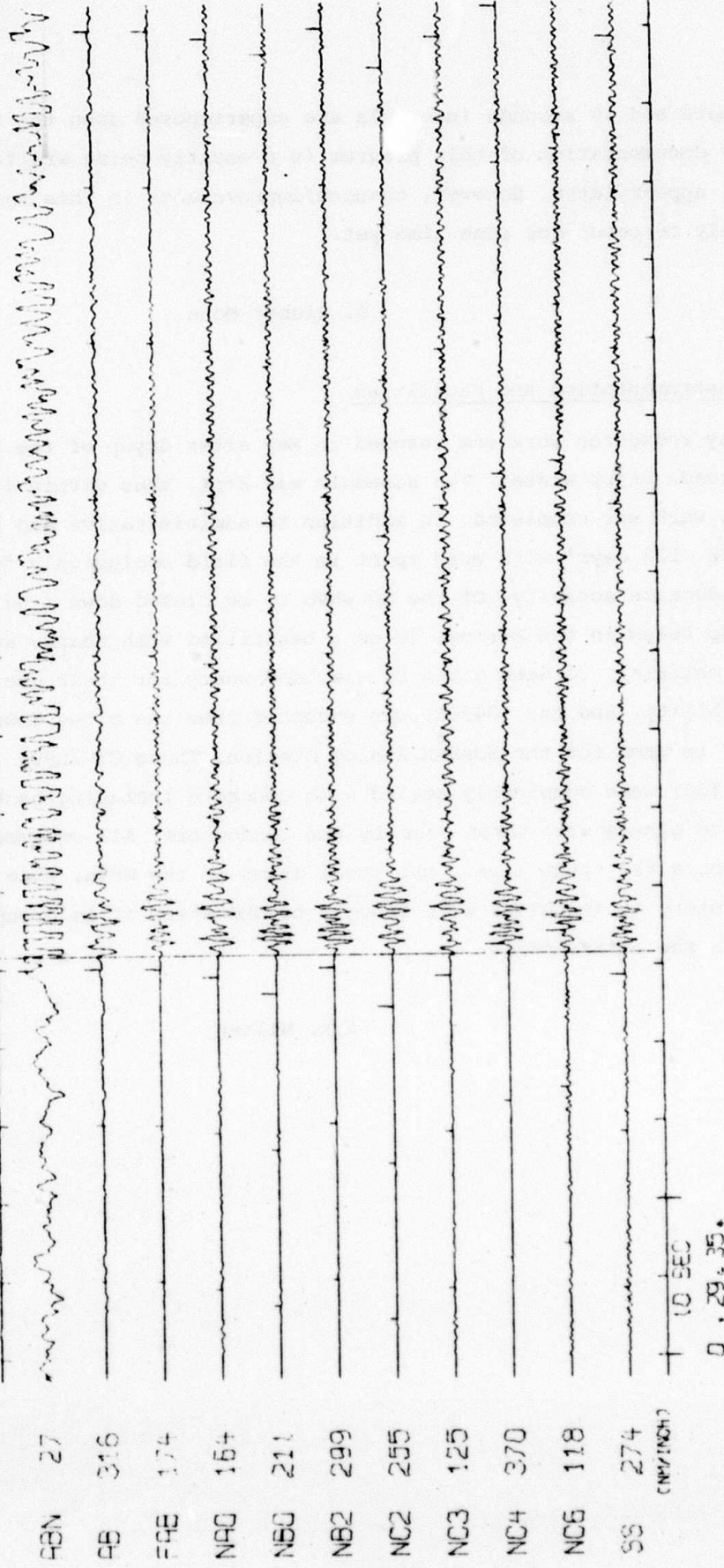


Fig. III.2.1 Event Plot Generated by AUTOEP.

IV. MAINTENANCE ACTIVITY

A brief review of the maintenance accomplished at the subarrays by the field technicians as a result of the remote array monitoring and routine inspections is given. The monitoring schedule has not been changed in the period. Except for the array reduction work, which has been the main workload during this period, all maintenance referred to is on the new array configuration.

Maintenance Visits

Fig. IV.1 shows the number of visits to the subarrays in the period. The subarrays have on the average been visited 4.2 times. The subarrays in the new array configuration have been visited 4.9 times on the average (excluding 06C, 3.8 times), the large number of visits to 06C are due to troubles with the SLEM giving noisy or no seismic data, and cable breakages (5 times).

There have been no maintenance visits on the communications system in the period.

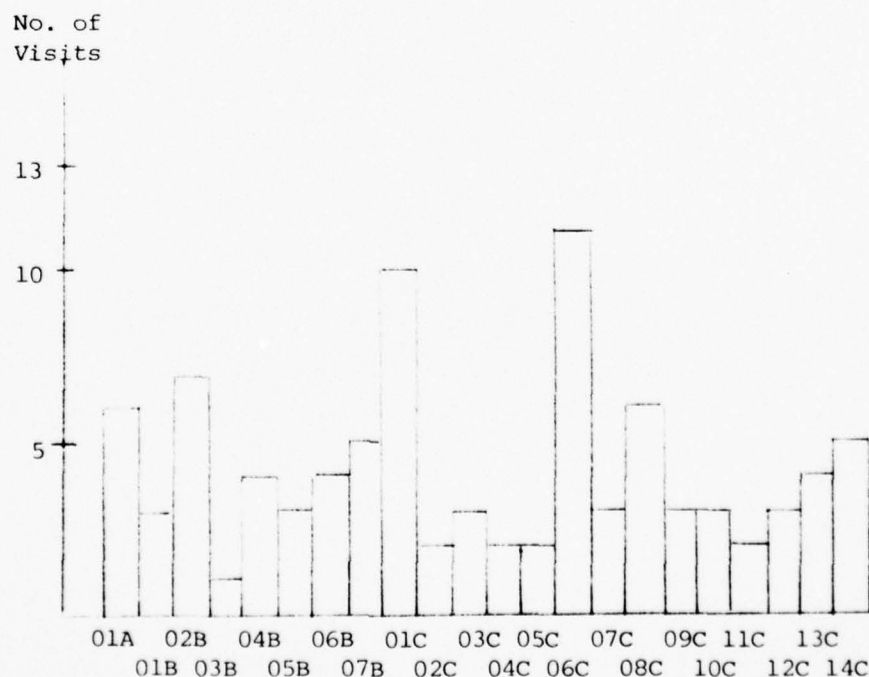


Fig. IV.1 Number of visits to NORSAR subarrays in the period 1 April-30 September 1977.

Preventive Maintenance Projects

The preventive maintenance work in the new array is described in Table IV.1.

Table IV.1
Preventive Maintenance Work in the Period
1 April - 30 September 1977

Unit	Action	No. of Actions
LTA	Adjustment of DC offset	31
	SP	4
	LP	
	Adjustment of channel gain	7
	SP	2
	LP	
Seis- mometer	MP adjustment (in field)	6
SLEM	BB adjustment	1
Power	Battery replacement due to aging of acid	6

Disclosed Malfunctions on Instrumentation and Electronics

Table IV.2 gives the number of accomplished adjustments and replacements of field equipment in the array with the exception of those mentioned in Table IV.1.

Table IV.2

Total number of required adjustments and replacements in the NORSAR data channels and SLEM electronics
(1 April - 30 September 1977)

Unit	Characteristic	SP		LP	
		Repl.	Adj.	Repl.	Adj.
Seis- mometer	RCD			6	
	MP (field)				5
	FP (field)				4
Seism. Ampl.	Distortion	2			
LTA	DCO		2		1
	Ch. gain		3		2
	CMR	1			
SLEM					
BB Gen.		2	1		
RSA/ADC		2	1		
EPU		2	1		
DU		1			
AU		1			

Malfunction of Rectifiers, Power Loss, Cable Breakages

Malfunction of the rectifiers is reported in Table IV.3. The number of cable breakages were three, requiring 17 days' work by the field technicians.

Table IV.3
Rectifier Malfunctions

Sub-array	Fault	Period of Inoperation	Comments
01B	Rectifier continuous in high charge	None	Timer fault
04C	Rectifier: No high charge	6-11 July	Trafo M2 burned defective U2 card

Conclusion

Satisfactory and stable performance and operation of the array instrumentation is observed also through this period. Due to the high priority given to the array reduction work, there are in some cases a small increase in the interval between time fault observed and time repaired. At the end of the last period the SP array average DC offset was -4 millivolts, but as a result of the preventive maintenance routines, this bias is now reduced to 0. The LP array average offset is -1 millivolts.

A.K. Nilsen

ABBREVIATIONS

ADC	-	Analog-to-Digital Converter
AU	-	Analog Unit
BB	-	Broad band
CMR	-	Common mode rejection
CTV	-	Central Terminal Vault
DC	-	Direct current
DCO	-	DC offset
DU	-	Digital Unit
EPU	-	External Power Unit
FP	-	Free Period
LP	-	Long period
LPV	-	Long period vault
LTA	-	Line Termination Amplifier
MP	-	Mass position
NMC	-	NORSAR Maintenance Center
RCD	-	Remote centering device
RSA	-	Range switching amplifier
SLEM	-	Seismic short and long period electronics module
SP	-	Short period
WHV	-	Well head vault

V. DOCUMENTATION DEVELOPED

V.1 Reports, Papers

Bungum, H. (1977): Semiannual Technical Summary, 1 October 1976-31 March 1977, NORSAR Sci. Report 2-76/77, NTNF/NORSAR, Kjeller, Norway.

Husebye, E.S., and I.B. Ramberg (1977): Geophysical Investigations, Norges Geol. Unders., Trondheim, Norway (in press).

Husebye, E.S., F. Ringdal, O.A. Sandvin and A. Christoffersson (1977): Statistical test theory in the analysis of macroseismic questionnaires, Tectonophysics (Special Issue), (in press).

Rieber-Mohn, D. (1977): Report from participation in the online conference on data communications networks, London, 9-11 May 1977, NORSAR Internal Report 1-76/77, NTNF/NORSAR, Kjeller, Norway.

Ringdal, F., E.S. Husebye and J. Fyen (1977): Earthquake detectability estimates for 435 globally distributed seismograph stations, PEPI Letter Section, (in press).

Sandvin, O.A., and D. Tjøstheim (1977): Multivariate autoregressive representation of seismic P-wave signals, submitted for publication.

Tjøstheim, D. (1977) Measuring deviations from stationarity, submitted for publication in Applied Probability.

Tjøstheim, D. (1977): A new measure of association for spatial variables, submitted for publication.

Tjøstheim, D. (1977): Multiplicity theory for random fields using quantum mechanical methods, Invited paper to be included in Springer Lecture Notes Series, (in press).

L.B. Tronrud

V.2 Program Documentation

No program documentation has been written during this period.

D. Rieber-Mohn

VI. SUMMARY OF SPECIAL TECHNICAL REPORTS/PAPERS PREPARED

VI.1 Interference of Surface Waves

A seismic array such as NORSAR is well suited for the study of interference of surface waves which arrive at the array from more than one direction. However, there is a severe limitation in the fact that traditional array analysis methods such as the high-resolution frequency-wavenumber analysis technique (Capon, 1969) cannot resolve two wave trains when they arrive simultaneously from two directions (Bungum and Capon, 1974).

The alternative analysis technique presented here is based on studying the effect of the interference on the envelope of the resulting wave trains observed over the array. To this end, we start with a monochromatic wave with amplitude A , angular frequency ω and angular wavenumber vector \bar{k} , which at a station with position vector \bar{r} can be represented by the expression

$$X(t) = A \exp[i(\omega t - \bar{k} \cdot \bar{r})] \quad (1)$$

If we add two such waves, with amplitudes A and $A(1-\epsilon)$ and wavenumber vectors \bar{k}_1 and \bar{k}_2 , respectively, it can be shown that the sum can be represented by the expression

$$X_s(t) = 2A \left[\cos \lambda - \frac{\epsilon}{2} \exp(i\lambda) \right] \exp[i(\omega t - \bar{k}^* \cdot \bar{r})] \quad (2)$$

where

$$\lambda = \frac{\bar{k}_1 - \bar{k}_2}{2} \cdot \bar{r} \quad , \quad \bar{k}^* = \frac{\bar{k}_1 + \bar{k}_2}{2}$$

For equal amplitude ($\epsilon=0$) the expression is reduced to the more familiar one used for example by Bungum and Capon (1974). From equation (2) it can now be found that the (normalized) power loss in dB due to interference can be expressed as

$$\text{Loss(dB)} = -10 \log_{10} \left[\frac{(1-\epsilon) \cos^2 \lambda + \left(\frac{\epsilon}{2}\right)^2}{1-\epsilon + \left(\frac{\epsilon}{2}\right)^2} \right] \quad (3)$$

If we now define x as the projection distance between seismometer and array center, measured along the resultant wave front, we find that

$$\lambda = |\bar{k}^*| \cdot x \cdot \text{tg} \left(\frac{\alpha}{2} \right) \quad (4)$$

where α is the angle between the two interfering wave trains. It now follows that the power loss can conveniently be plotted as a function of the quantity $|\bar{k}^*| \cdot x$, given in radians.

For an initial testing of the interference pattern measured in this way at NORSAR, we have used a single seismometer recording of an earthquake from Japan. This recording has been used to simulate the simultaneous arrival of two wave trains with the same phase velocity (3.8 km/s), but with different azimuths (expressed through α) and amplitudes (expressed through ϵ). The measurements have been made at a period of 30 sec, and are based upon computation of the envelope for each of the 22 long period seismometer recordings at NORSAR. Fig. VI.1.1 here shows the effect of keeping a constant amplitude ratio of 1:1 while varying the azimuth difference from 30° to 120° , whereas Fig. VI.1.2 shows the results of keeping the azimuth difference constant ($\alpha=60^\circ$) while varying the amplitude ratio from 1:1 to 10:1. It is seen from these figures that there is a very good fit between measured and predicted power loss, and from the results we can draw the following conclusions, valid for 30 sec period surface waves recorded at an array with the size of NORSAR (diameter about 110 km):

- 1) The power loss due to interference is not serious for azimuth differences of 30° or less. At 60° , the loss may be as large as 20 dB.
- 2) The power loss due to interference is significant down to an amplitude ratio of about 5:1, although detectable at a ratio of 10:1.

H. Bungum

A. Levshin, Inst. Physics of the Earth,
Moscow

References

- Bungum, H., and J. Capon (1974): Coda pattern and multipath propagation of Rayleigh waves at NORSAR, Phys. Earth Planet. Inter., 9, 111-127.
- Capon, J. (1969): High-resolution frequency-wavenumber spectrum analysis, Proc. IEEE, 57, 1408-1418.

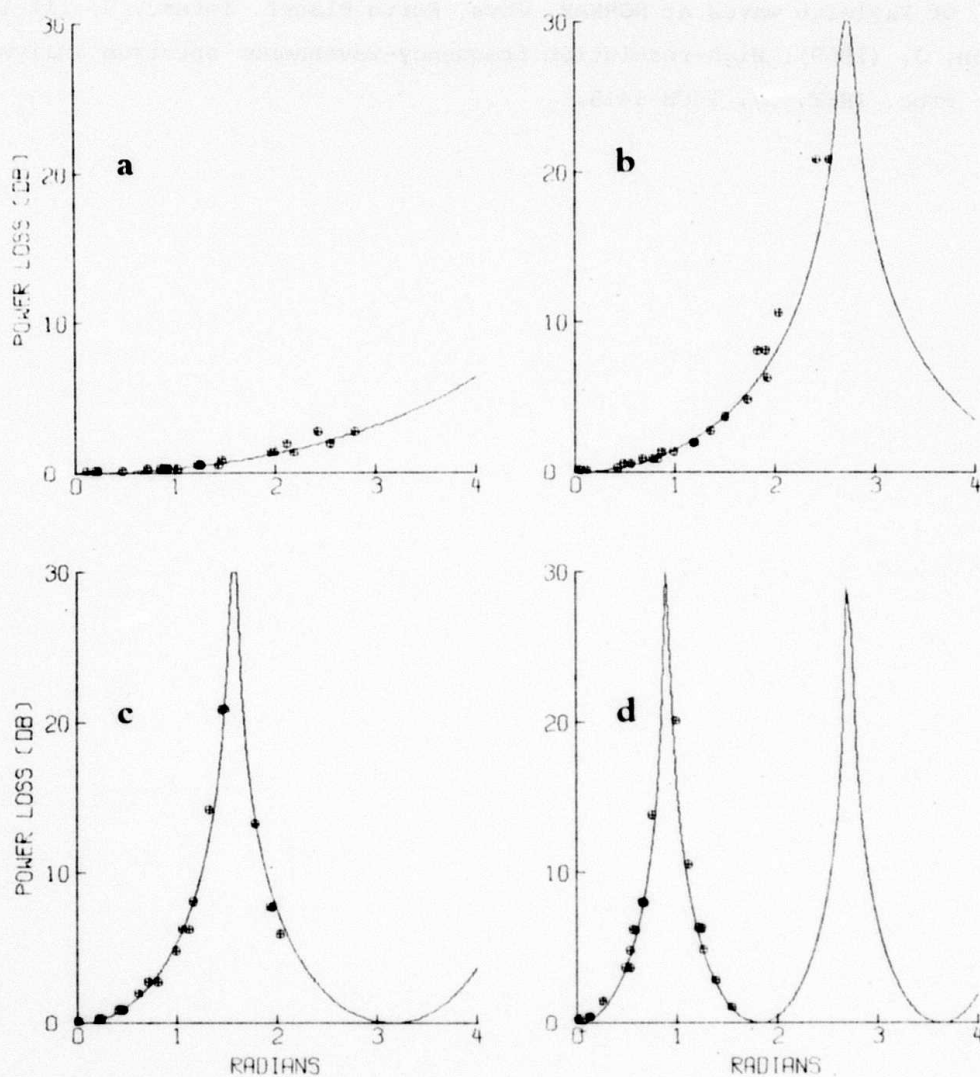


Fig. VI.1.1 Theoretical and observed power loss due to interference between two surface wave trains of equal amplitude arriving with an azimuth difference of a) 30° , b) 60° , c) 90° and d) 120° .

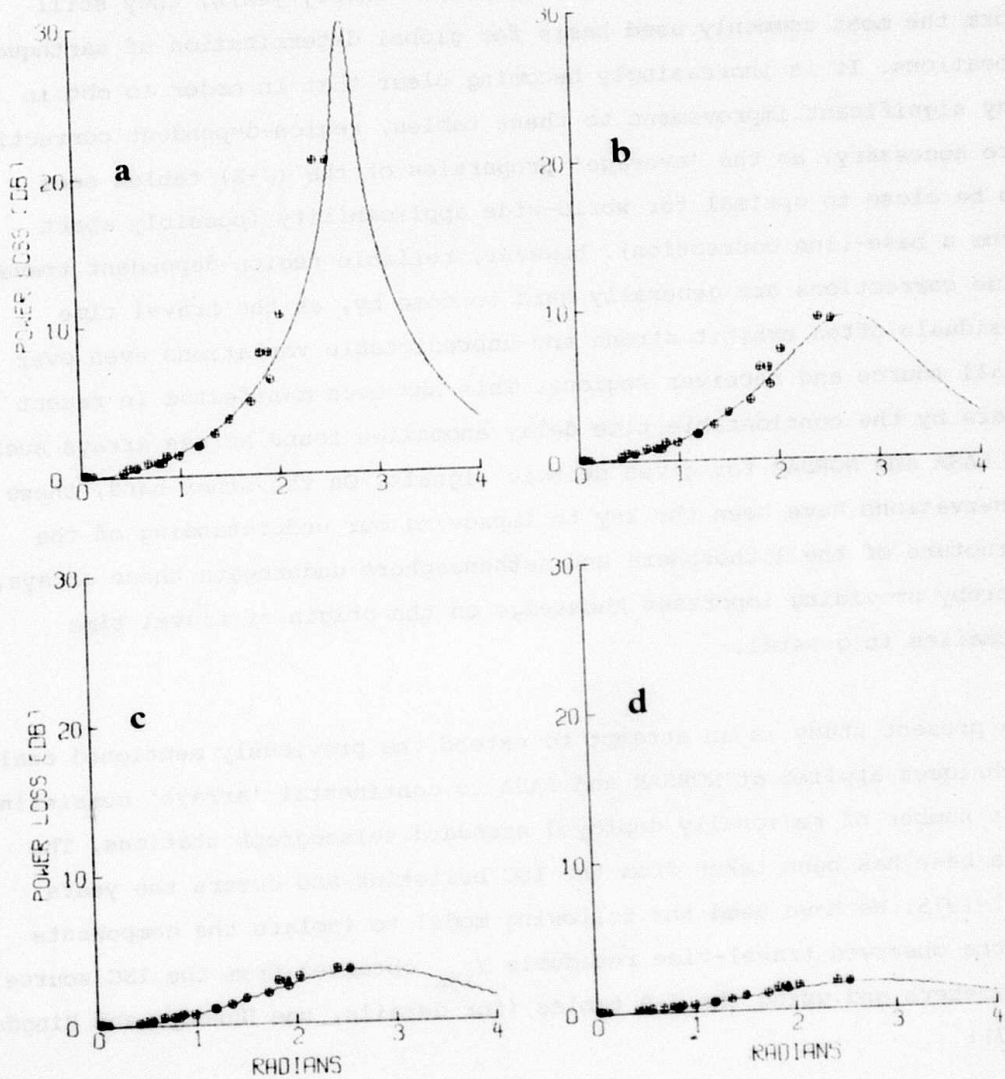


Fig. VI.1.2 Theoretical and observed power loss due to interference between two surface wave trains with an azimuth difference of 60° , and with amplitude ratios of a) 1:1, b) 2:1, c) 5:1 and d) 10:1.

VI.2 P-wave Travel Time Studies using a Continental Array

Although the Jeffreys-Bullen (J-B) tables for travel times of seismic waves have been in existence for more than thirty years, they still form the most commonly used basis for global determination of earthquake locations. It is increasingly becoming clear that in order to obtain any significant improvement to these tables, region-dependent corrections are necessary, as the 'average' properties of the (J-B) tables seem to be close to optimal for world-wide applicability (possibly apart from a base-line correction). However, reliable region-dependent travel-time corrections are generally hard to come by, as the travel time residuals often exhibit strong and unpredictable variations even over small source and receiver regions. This has been manifested in recent years by the considerable time delay anomalies found across arrays such as LASA and NORSAR for given seismic signals. On the other hand, these observations have been the key to improving our understanding of the structure of the lithosphere and asthenosphere underneath these arrays, thereby providing important knowledge on the origin of travel time anomalies in general.

The present study is an attempt to extend the previously mentioned analysis techniques applied at NORSAR and LASA to continental 'arrays' consisting of a number of regionally deployed standard seismograph stations. The data base has been taken from the ISC bulletins and covers the years 1971-1975. We have used the following model to isolate the components of the observed travel-time residuals Y_{ijk} obtained from the ISC source parameters and using the J-B tables (for details, see Husebye and Ringdal, 1977):

$$Y_{ijk} = R_{ik} + S_k + \gamma_{jk} + \epsilon_{ijk} \quad \begin{array}{ll} i = i\text{-th station} & (1) \\ j = j\text{-th event} \\ k = k\text{-th source region} \end{array}$$

where:

- R_{ik} denotes near-receiver effects and varies by station and region, but is assumed constant for events within a (small) source region

- S_k denotes source effects and is, for a given event and region, assumed constant for all stations within the network. The variations of source effects within a given source region are considered random and included in the term γ_{jk} , which is assumed to be normally distributed. Note that γ_{jk} will include apparent 'source effects' that are due to, e.g., possible mislocations of the events or erroneous origin time.
- ϵ_{ijk} is a normal random variate that incorporates effects not previously accounted for, such as inherent uncertainties in the travel time estimates caused by small-scale perturbations along the ray path. Possible minor errors in the reading of signal arrival times at different stations are also included in this term, while larger errors in these readings have been avoided by excluding all observed residuals of more than 5 seconds in absolute value.

We should like to comment on the physical realization of the R_{jk} -term which is tied to a 2-D modelling of structural heterogeneities in the lithosphere beneath the receiver. It is here assumed that these anomalies are restricted to a layer of thickness of the order of 30-50 km at the bottom of the lithosphere which thickness is typically 150-200 km within continental areas. The mentioned assumed heterogeneous layer is in turn subdivided into blocks, the areal extent of which is typically 15 x 15 km. The source regions are indirectly defined via this block pattern, in such a way that each source region comprises those events whose ray path to the center station of the network penetrates a given block. The above approach is a viable alternative approach to the more complicated 3-D modelling of Aki et al (1976, 1977), which in practice is restricted to the dense sampling of large aperture seismic arrays and similar networks as demonstrated by Haddon and Husebye (1977, see also section VI.3).

The model (1) is made complicated by the effect of missing observations, which in fact occur frequently when using ISC data. For example, when considering a network of 15-20 stations in Fennoscandia, the number of available observations for a given event would very seldom exceed 5-10. For this reason, the solution of (1) must take missing observations into account.

Referring to Husebye and Ringdal (1977) for details, Fig. VI.2.1 shows a 'Fennoscandian continental network' of 17 stations used in conjunction with the present model. Note that NORSAR is included in this network, but only as a single station, i.e., only the observed absolute arrival times at instrument 01A01 are used in the present context. Fig. VI.2.2 shows the pattern of residual terms R_{ik} obtained for NORSAR when applying the model (1) to the Fennoscandian network. For comparison, Fig. VI.3.2a shows a corresponding pattern of anomalies obtained by Haddon and Husebye (1977) using NORSAR data only, i.e., using NORSAR as an array station. The correspondence between the two figures is seen to be excellent. The apparent baseline shift between the two patterns is not important in the present context, as the baseline correction is arbitrarily defined as zero in Fig. VI.3.2a. Thus it has been demonstrated that the simple model (1) may indeed be used to extract information on the underlying structure of single seismograph stations. Moreover, our results suggest that the quality of this information, at least as concerns gross structures, will be comparable to that obtainable by analyzing time delay residuals from seismic arrays. Of course, it is necessary in this respect to have a suitable network nearby in order to apply (1) and eliminate 'average' source effects. We plan in the near future to conduct similar analyses for various subsets of the global network of stations reporting to the ISC, and also combine the resulting structures into more large-scale patterns wherever possible.

E.S. Husebye

F. Ringdal

References

- Aki, K., A. Christoffersson and E.S. Husebye (1976): Three-dimensional seismic structure of the lithosphere under Montana LASA, Bull. Seism. Soc. Amer., 66, 501-524.
- Aki, K., A. Christoffersson and E.S. Husebye (1977): Determination of the three-dimensional seismic structure of the lithosphere, J. Geophys. Res., 82, 277-296.

Haddon, R.A.W., and E.S. Husebye (1977): Joint interpretation of P-wave travel time and amplitude anomalies in terms of 2-D lithospheric heterogeneities, Manuscript in preparation.

Husebye, E.S., and F. Ringdal (1977): 2-D heterogeneities in the lithosphere and the concept of continental arrays in analysis of ISC time residuals, Manuscript in preparation.

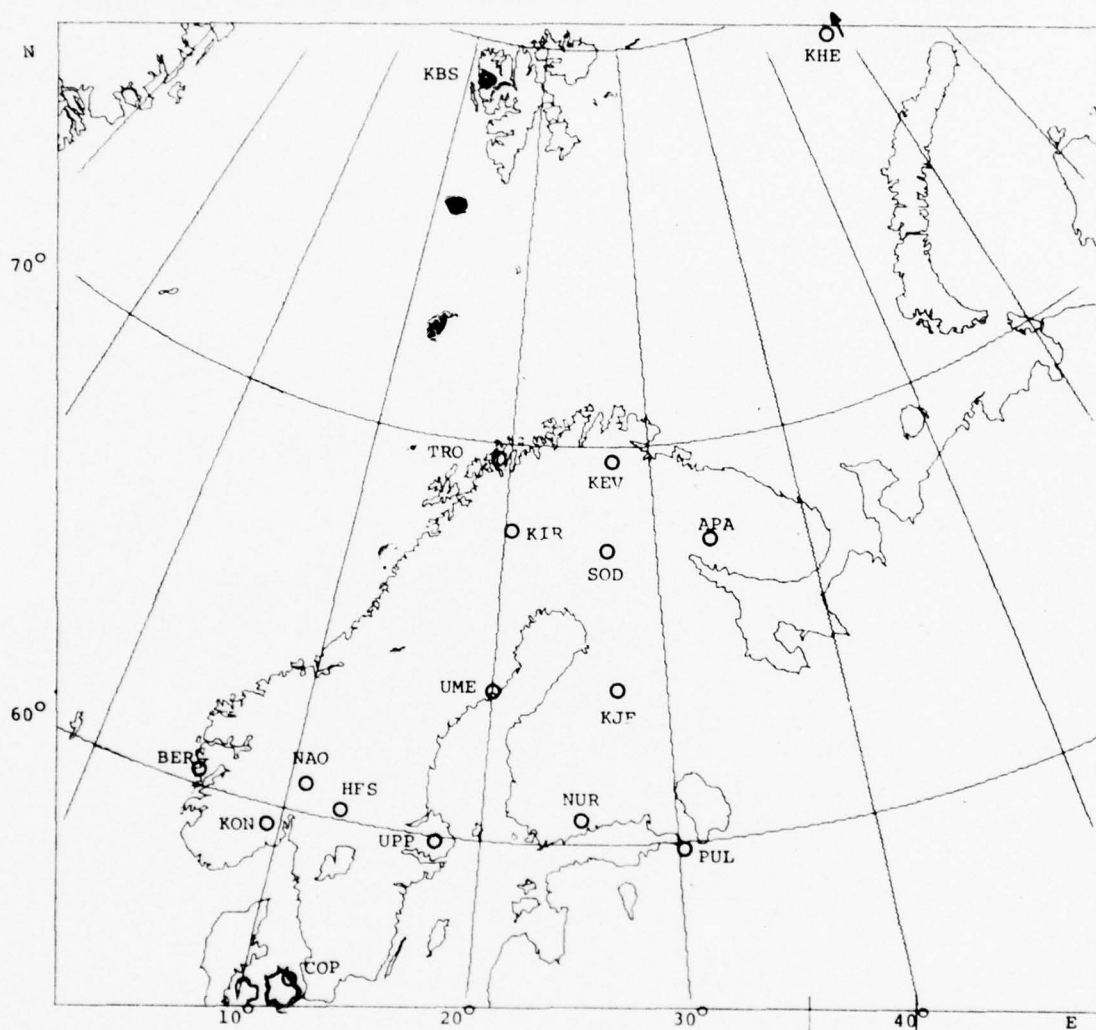


Fig. VI.2.1 Location of stations within the extended Fennoscandian continental array used in this study.

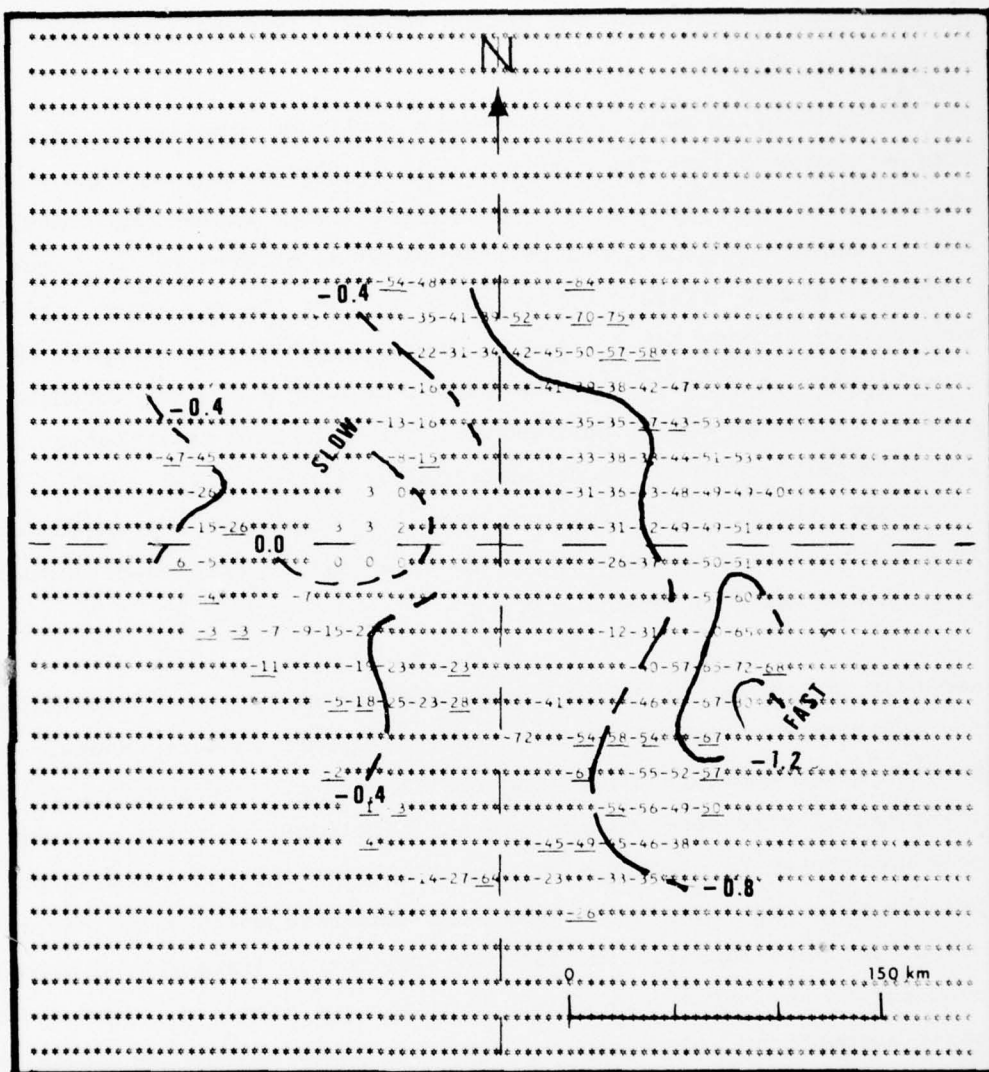


Fig. VI.2.2 NORSAR travel time residuals derived from ISC-data files using the continental array shown in Fig. VI.2.1. The given numbers are in units of 1/50 sec, except for the time residuals associated to the contours which are specified in seconds. The time anomaly pattern presented here (and derived from absolute time observations) is in good agreement with similar results presented in Fig. VI.3.2a (and derived from relative time observations). Although areas of slow and fast structures are almost coincident, a flat baseline shift of approx. 0.5 sec is apparent. The non-uniqueness in estimating this parameter is discussed in detail in Husebye and Ringdal (1977).

VI.3 P-wave Amplitude Observations Across NORSAR - Observational and Theoretical Results

The variability in short period P-wave amplitude observations has intrigued seismologists for many years as manifested through the numerous magnitude scales proposed and amplitude-distance tables published. Better sampling of this kind of phenomenon as offered by the large aperture seismic arrays clearly indicates that the mentioned amplitude variability is more severe than generally assumed. For example, amplitude variations amounting to one magnitude unit are often observed across the NORSAR array. Furthermore, the amplitude distribution is approximately lognormal as demonstrated by Ringdal et al (1975). Intuitively, the reported amplitude anomalies must have a counterpart in structural heterogeneities in the array siting area, and this is the problem addressed in this study.

Recently Aki et al (1977) have developed a flexible block modelling procedure for estimating deterministically the 3-D seismic velocity anomaly structure beneath large aperture arrays and similar types of seismograph networks using travel time observations. To our knowledge, no similar study has been undertaken to interpret extensive P-wave amplitude anomalies. This is perhaps not surprising as at least the NORSAR-reported amplitude anomalies often vary very rapidly with changing epicentral distance and azimuth in contrast to the relatively slowly varying time anomalies. Some of the basic assumptions underlying our approach to tackle the amplitude problem are as follows (reference array is NORSAR):

- In the context of P time and amplitude anomalies, the postulated inhomogeneous layer can be treated as an equivalent thin lens located at the depth D.
- The scales of the anomalies are such that ray theory is applicable.

The wave equation in analysis of time-derived lens models

Assuming slowly varying physical properties, the acoustic wave equation is applicable (for details, see Claerbout, 1976):

$$p_{xx} + p_{yy} + p_{zz} - c^2 p_{tt} = 0 \quad (1)$$

where p denotes pressure variations in the medium, c is velocity and the subscripts denote partial derivatives. For $c = \text{constant}$ a solution of (1) corresponding to a plane harmonic wave travelling in the z direction is

$$p' = p_0 e^{i(mz - \omega t)} \quad (2)$$

where $m = \omega^2/c^2$ is the wavenumber and $p_0 = \text{constant}$.

Now, a solution of (1) may be sought which has the form (2) but with p_0 now a slowly varying function of position in the medium. Substituting (2) into (1) and dropping the zero subscript then gives

$$p_{xx} + p_{yy} + p_{zz} + 2imp_z - m^2 p + p\omega^2/c^2 = 0 \quad (3)$$

If the ray deflections are small, the pressure (or equivalent amplitude) modulation p will be slow and the term p_{zz} will be relatively small. Ignoring the latter term, we get:

$$p_z = \frac{1}{2\pi} (p_{xx} + p_{yy} + \epsilon m^2 p) \quad (4)$$

where $\epsilon = (\omega^2/m^2 c^2 - 1)$ and $c = c(x, y, z)$.

Equation (4) is easily solved using finite difference methods. The boundary conditions to be applied on the artificial grid boundaries are somewhat arbitrary and are here chosen as zero slope.

Calculation of time delays from amplitudes for a thin lens

Consider a plane wave with uniform amplitude p_0 moving vertically upwards and passing through the horizontal thin lens L in the plane $z = 0$. The wavefront advances in the direction of the rays which in the vicinity of each point on the wavefront converge or diverge. Let ρ_1, ρ_2 denote the two principal radii of curvature at point $p(x, y, z)$ on the wavefront and let ξ, η be local cartesian coordinates in the z -plane corresponding

to the principal planes of curvature at P. From ray theory we have that the energy flux through the area ABCD and EFGH (see Fig. VI.3.1) are equal, thus

$$p^2/p_0^2 = (\text{AREA})_{ABCD}/(\text{AREA})_{EFGH} = \frac{\rho_1^{+R}}{\rho_1} \cdot \frac{\rho_2^{+R}}{\rho_2} \quad (5)$$

where R is the mean distance from the lens. The principal radii of curvature are given by

$$1/\rho_1 = r_{\xi\xi} \quad ; \quad 1/\rho_2 = r_{\eta\eta} \quad (6)$$

where r is the advance of the wavefront from the lens. Substituting into (5) gives

$$r_{\xi\xi} + r_{\eta\eta} + Rr_{\xi\xi}r_{\eta\eta} = (p^2/p_0^2 - 1)/R \quad (7)$$

Transforming to cartesian coordinates:

$$r_{xx} + r_{yy} + R\{r_{xx}r_{yy} - (r_{xy})^2\} = (p^2/p_0^2 - 1)/R \quad (8)$$

This differential equation, together with suitable boundary conditions, determines the shape of the wavefront in terms of the relative amplitudes at distance R from the lens. If $|\frac{R}{\rho_1}|$ and $|\frac{R}{\rho_2}|$ are small the nonlinear terms may be neglected. The equation then becomes Poisson's equation which has a unique solution within a given region if r is specified on its boundary. If $|\frac{R}{\rho_1}|$ and $|\frac{R}{\rho_2}|$ are moderate, the nonlinear terms may be transferred to the right-hand side of the equation and treated as perturbation terms. The nonlinear equation can then be solved using standard techniques.

Derivation of thin lens models

Projection of travel time data.

The travel time data we have used consist of relative arrival times at each of NORSAR's 22 subarrays for about 180 seismic event locations in the distance range 25° - 135° . This set includes those of Berteussen (1974) together with an additional 90 events to obtain an improved coverage of certain azimuth sectors. If the true directions of approach of rays at

surface receivers were known, the relative time delays required to be produced by the hypothetical thin lens could be obtained by projecting the observed delays back to points on the lens where corresponding rays passed through. We have used the NORSAR least squares plane wavefront direction as the ray approach direction at each subarray for each event. The relative time delays to be produced by the lens are determined by projecting the observed delays to the plane of the lens using the NORSAR direction. A thin lens model thus constructed is shown in Fig. VI.3.2a and VI.3.2b. The errors associated with the approximation are of the order of 0.1 sec.

To summarize, simple thin lens models have been constructed which can account for about 80% of the mean square observed travel time anomalies. The optimum lens depth is found to be around 150 km though depths of between 100 and 200 km satisfy the time delay data almost equally well.

Projection of amplitude data

Direct comparison of amplitude data with theoretical results for individual events is hardly warranted because of the small-scale variability of observed amplitudes and the large number of cases involved. For these reasons it is desirable to smooth the data and also reduce the number of comparisons that need to be made. For a simple lens-type structure this may be done by projecting the amplitude data (taken from Berteussen and Husebye, 1974) in essentially the same way as for the times (notice that lens models give similar surface amplitude distributions for similar arrival directions apart from the horizontal translations involved). A single theoretical amplitude distribution can therefore be used for comparison with data for a range of different arrival directions. Equivalently, the theoretical amplitude distribution may be kept fixed and the data translated. The relative data translations required to correspond to results for a thin lens are given simply by projecting the amplitude data onto the plane of the lens in precisely the same manner as for the times. It is, of course, necessary in this case to introduce appropriate amplitude scaling factors (additive constants) for each event. The results obtained (see Fig. VI.3.3) show that the method works surprisingly well for the entire range of the available data. Also for the amplitude projections the best fitting projection depths are around 150-200 km.

Comparison of amplitude projections with theoretical amplitudes for the lens models

In the context of the thin lens hypothesis, amplitude projections correspond to surface amplitudes for a wave of vertical incidence. The relationship between the amplitude and time observations may therefore be examined by comparing amplitude projections with theoretical ones for models derived from the time data. For example, comparison of Figs. VI.3.3 and VI.3.4 shows that while there are discrepancies in detail, the major features of the theoretical amplitude distribution are in good agreement with those observed, in that regions of relatively high and low amplitudes occur in similar locations in each figure. A major cause of the discrepancies of small wavelength features is that amplitudes depend essentially on the curvature of the wavefront induced by the lens, and quite small errors in the inferred time delays can result in large local disturbances in the associated amplitude pattern.

Lens models derived using amplitudes

With the same assumptions as in the previous section, amplitude projections may be interpreted as representing wave amplitudes for a vertically incident wave over an extensive area of the earth's surface. In this section we treat the amplitude projections in this way and apply Eq. (8) to derive corresponding lens models to fit these amplitude projections exactly. The difference between calculated and observed lens models is shown in Fig. VI.3.5, and the differences are indeed small except for a minor area in the northeast quadrant (the correlation between these two surfaces is 0.91!)

Discussion and conclusions

The results given above clearly demonstrate that medium-scale travel time and amplitude anomalies observed at NORSAR are strongly correlated. The physical structure responsible for both may be modelled by a single homogeneous layer at a mean depth of about 200 km beneath the array. We consider, for example, that our results on amplitudes provide strong support for the

hypothesis that the main travel time anomalies observed at NORSAR result almost entirely from 3-D structure which may be represented to a good first approximation as a 2-D 'layer' in the upper mantle or bottom of the lithosphere beneath the array.

In conclusion we remark that our lens models entail typical ray deflections of order 5° for each one-way transit through the upper mantle so that waves reflected from the earth's surface in the vicinity of NORSAR would be effectively scattered in a range of about $\pm 10^\circ$ from the mean ray direction. Such scattering is consistent with similar scattering effects in other regions of the upper mantle as indicated by observations and interpretation of the seismic phases PP and P'P' (see, e.g., King et al, 1975; Haddon et al, 1977). The results presented above demonstrate very clearly the inherent problems in properly estimating m_b -magnitudes.

R.A.W. Haddon, Univ. of Sydney
E.S. Husebye

References

- Aki, K., A. Christoffersson and E.S. Husebye (1977): Determination of the three-dimensional seismic structure of the lithosphere, J. Geophys. Res., 82, 277-296.
- Berteussen, K.-A. (1974): NORSAR location calibrations and time delay corrections, Sci. Rep. 2-73/74, NTNF/NORSAR, Kjeller, Norway.
- Berteussen, K.-A. (1977): Moho depth determinations based on spectral ratio analysis of NORSAR long period P-waves, Phys. Earth Planet. Inter., 15, 13-27.
- Berteussen, K.-A., and E.S. Husebye (1974): Amplitude pattern effects on NORSAR P-wave detectability, Sci. Rep. 1-74/75, NTNF/NORSAR, Kjeller, Norway.
- Claerbout, J.F. (1976): Fundamentals of Geophysical Data Processing, McGraw-Hill, New York.
- Haddon, R.A.W., and E.S. Husebye (1977): Joint interpretation of P-wave time and amplitude anomalies in terms of 2-D lithospheric heterogeneities, manuscript in preparation.

Haddon, R.A.W., E.S. Husebye and D.W. King (1977): Origins of precursors to P'P', *Phys. Earth Planet. Inter.*, 14, 41-71, 1977.

King, D.W., E.S. Husebye and R.A.W. Haddon (1975): Precursors to PP, *Phys. Earth Planet. Inter.*, 10, 102-127.

Ringdal, F., E.S. Husebye and A. Dahle (1975): P-wave envelope representation in event detection using array data, *Proceedings, NATO Advanced Study Institute 'Exploitation of Seismograph Networks'* (K.G. Beauchamp, ed.), Nordhoff-Leiden, 353-372.

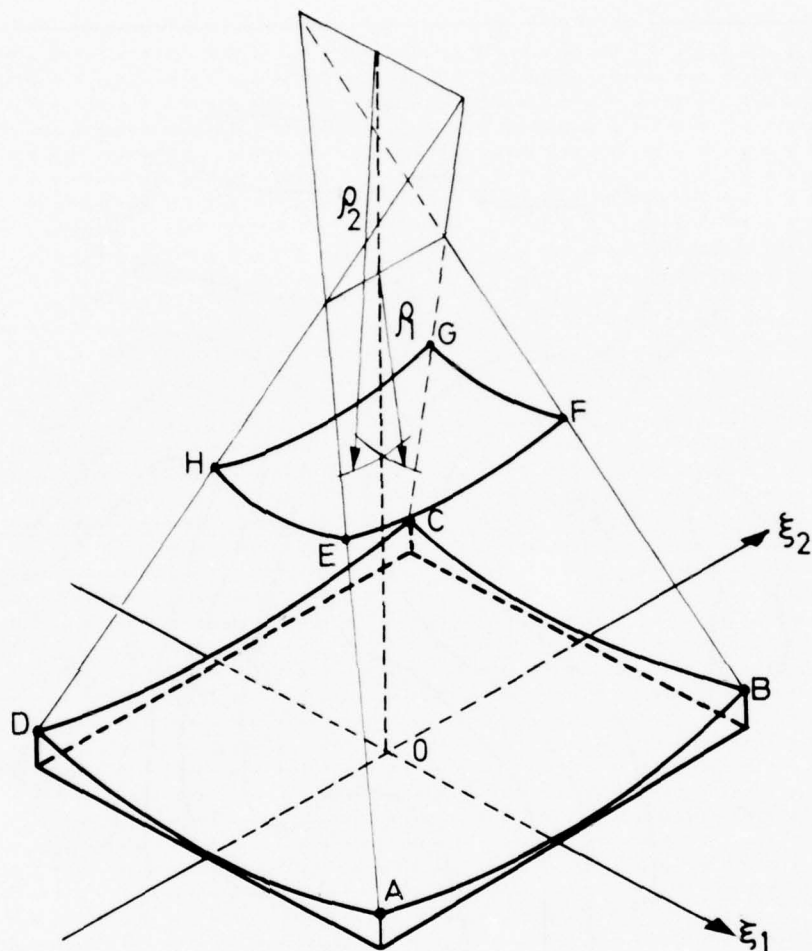


Fig. VI.3.1 Schematic illustration of focusing effect for a perturbed wavefront. The energy flux through the areas ABCD and EFGH is the same. The principal radii of curvature of the wavefront in the latter area are ρ_1 and ρ_2 . The rays in the vicinity of each point of the wavefront converge or diverge to or from the two centers of curvature as shown in the figure.

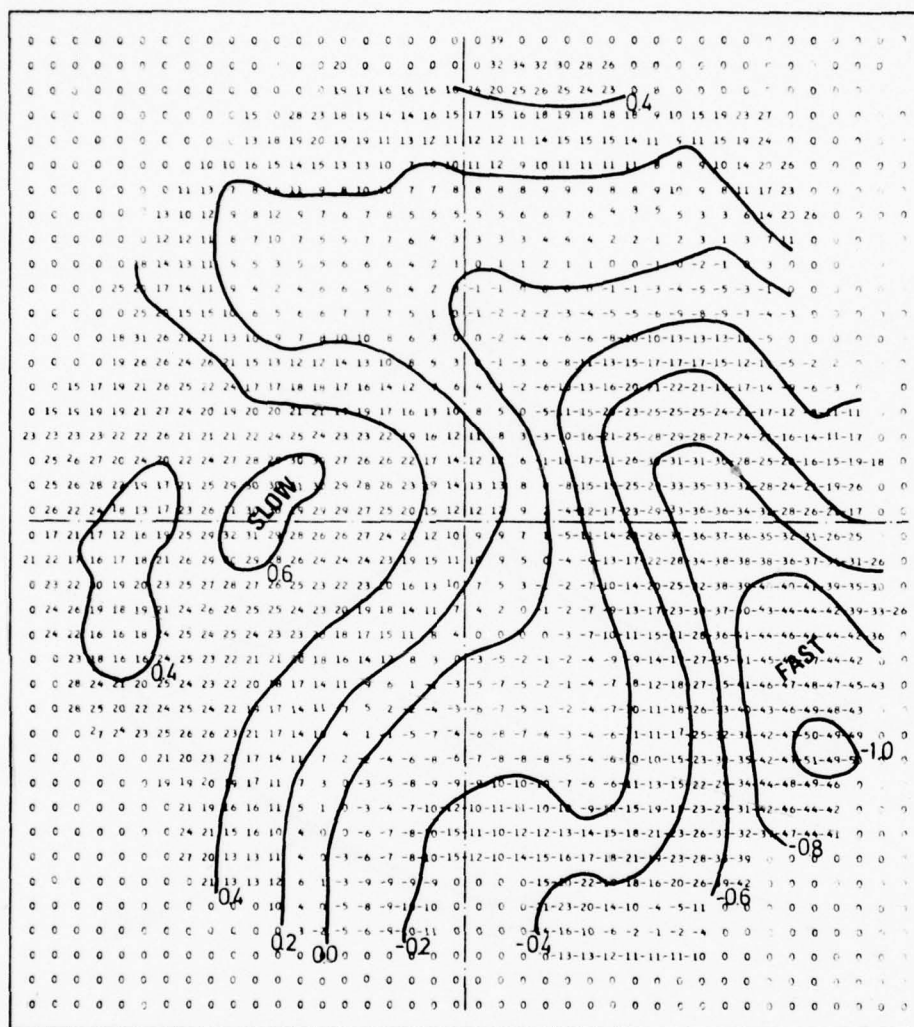


Fig. VI.3.2a Thin lens model for a depth of 150 km constructed by projecting and averaging travel time residuals as described in the text. The area shown is a 400 km x 400 km square whose center is located vertically below the center of the array. The numbers at each 10 km x 10 km grid point represent time delays produced by the lens at the point. For computer printing convenience the time values are in units of 0.02 sec, while the contouring intervals are unscaled. Note the systematic trend in time delays from positive on the left to negative on the right of the figure.

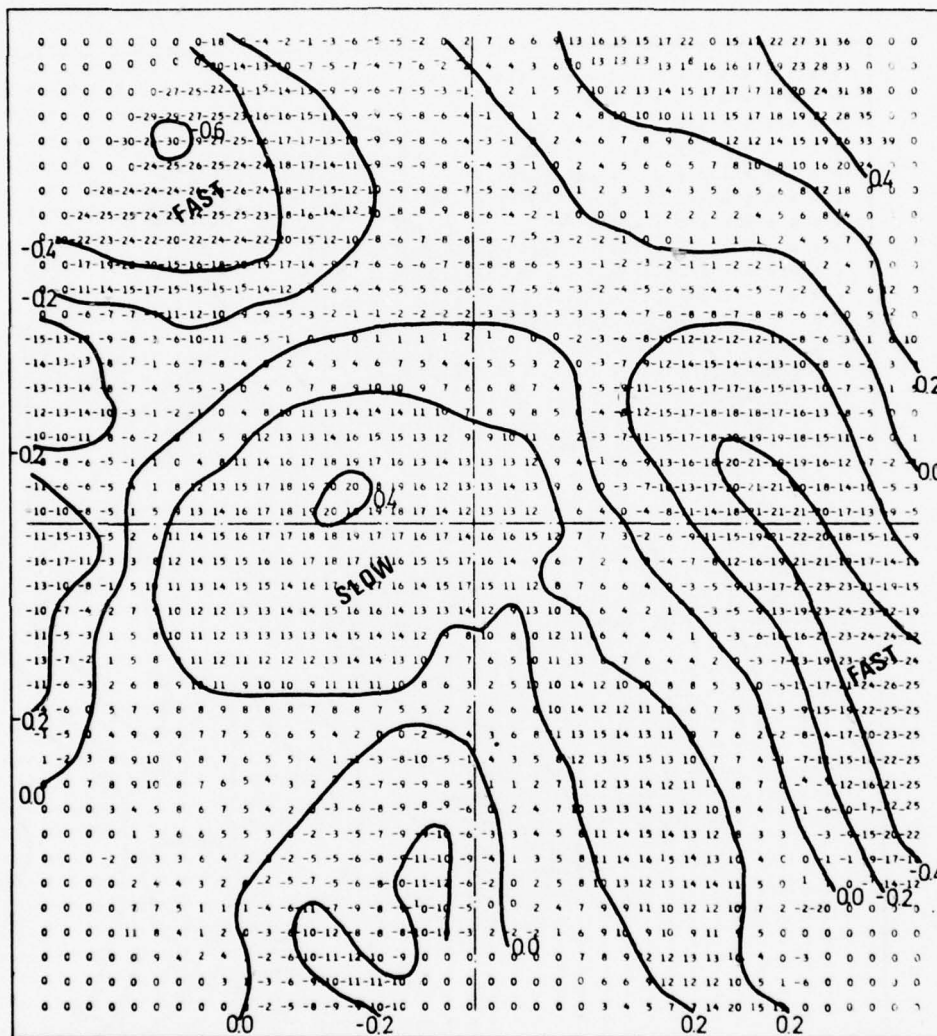


Fig. VI.3.2b Thin lens model for a depth of 200 km in which the systematic trend evident in Fig. VI.3.2a has been removed as described in the text. Other details as in caption for Fig. VI.3.2a.

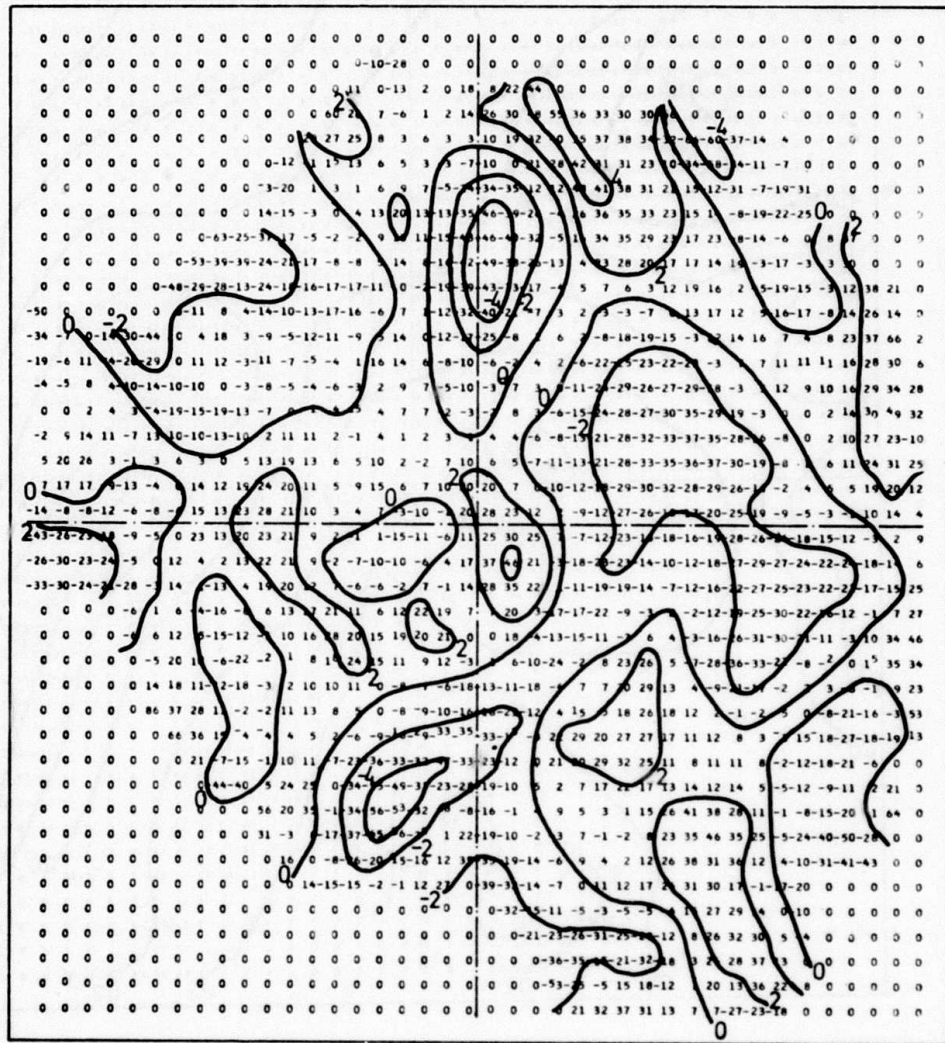


Fig. VI.3.3

Amplitude projection for D=200 km using the projection procedure described in the text. The numbers give amplitude values in dB multiplied by 10, while the contours are in non-scaled dB-units. Note the extensive regions of relatively high and low amplitudes.

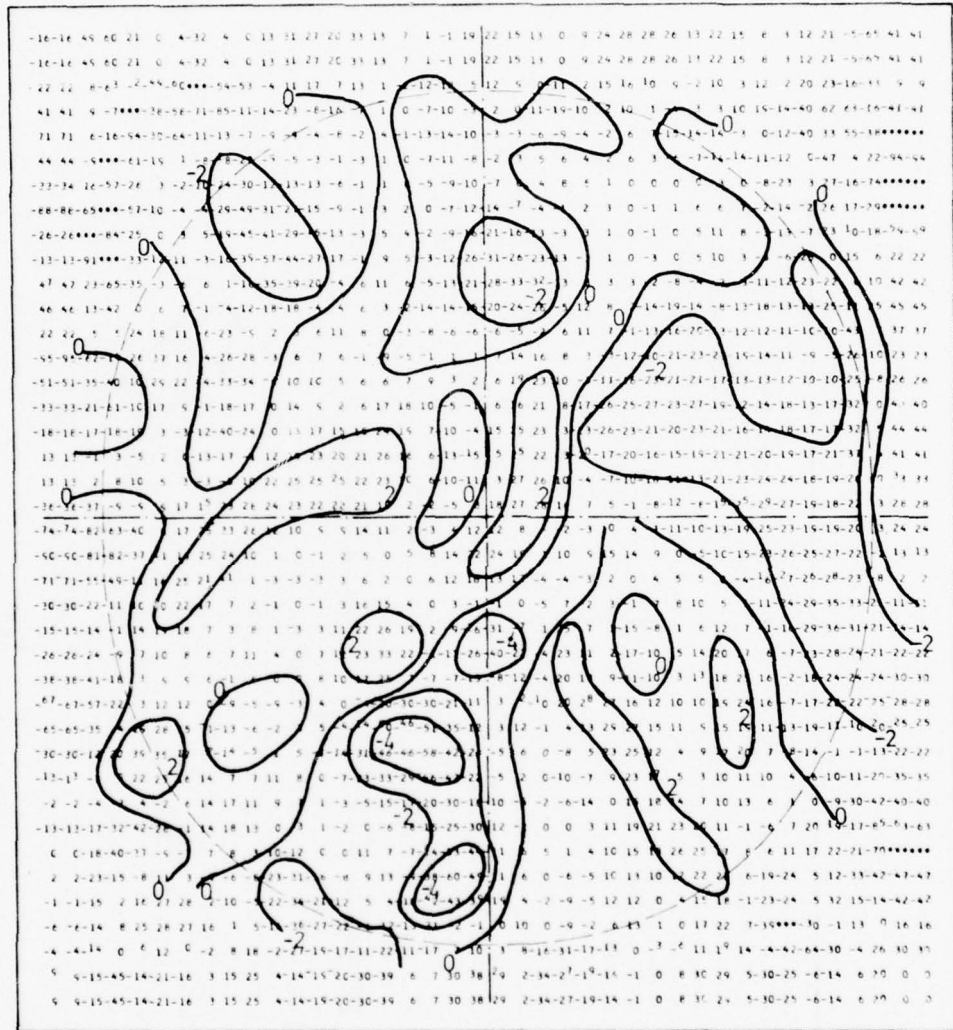


Fig. VI.3.4

Theoretical amplitudes for a wave of vertical incidence for the thin lens model shown in Fig. VI.3.2b. The amplitude values are in units of dB multiplied by 10, while the contours shown are in non-scaled dB-units. Note that the area outside the dashed circle in the figure should be disregarded because of spurious effects associated with the boundaries of the lens. Positive and negative values indicate relatively large and small amplitudes, respectively.

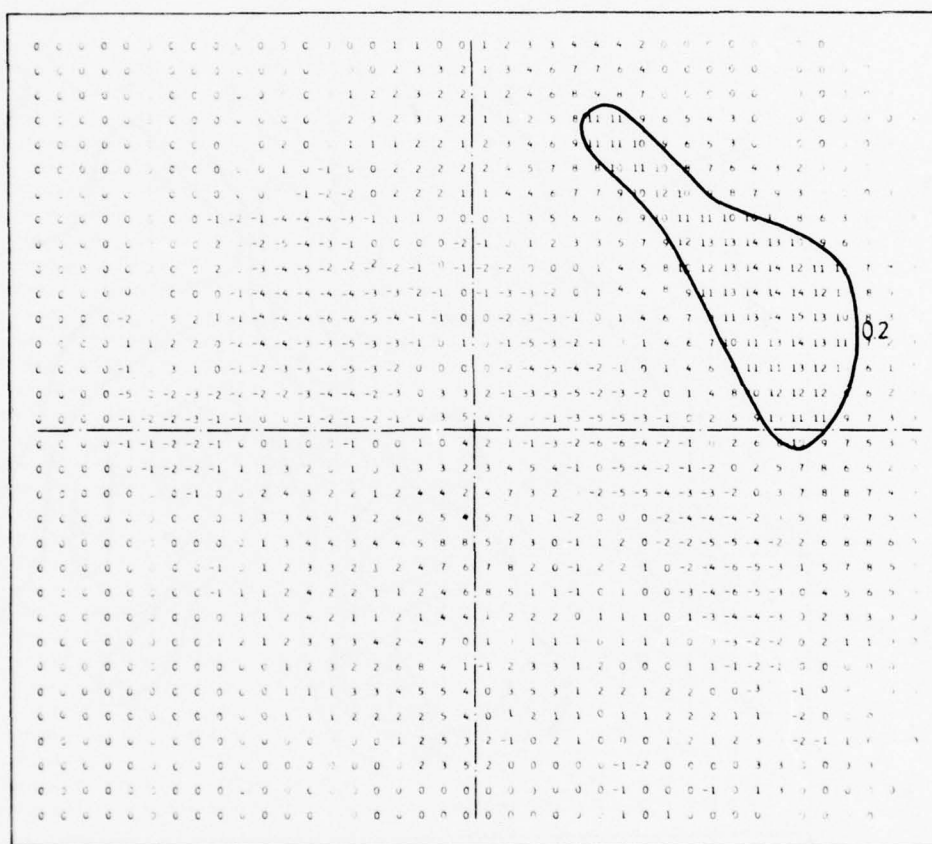


Fig. VI.3.5 Differences between corresponding grid point time delays for the lens models shown in Figs. VI.3.2b and those derived from Fig. VI.3.3. Note that with the exception of the northeast quadrant, the differences are small. This result implies that the travel time and amplitude anomalies may be jointly satisfied by a suitable thin lens model.

VI.4 Lateral P-velocity Distribution in the Upper Mantle Derived from NORSAR Data

An integral part of problems associated with discrimination between earthquakes and underground nuclear explosions is the composition of the upper mantle, in particular its P-velocity distribution. There are several approaches used for studying these kinds of problems, that is, inversion of surface wave data, seismic refraction profiling (very costly), various types of analyzing techniques in conjunction with seismic network data and so-called tau-inversion (Bessanova et al, 1974; Kennett, 1976) of gross P-wave travel time data. The latter two methods have been popular with NORSAR scientists in analysis of P-wave recordings at NORSAR from explosions in Western Russia and earthquakes in southeastern Europe (for references, see King and Calcagnile, 1976; and England, Worthington and King, 1977). More recently, England, Kennett and Worthington (1977) have undertaken a comprehensive analysis of NORSAR recordings from the North Atlantic, and the essence of their findings is to be reported here. We note in passing that NORSAR has a rather unique location being situated within 30 degrees from 3 major tectonic zones: the old shield of Western Russian platform, the young collision zone of SE Europe and the Alpine-Carpathian chain and the active spreading ridge of the North Atlantic Ocean.

A travel time curve for P seismic waves recorded at NORSAR from earthquakes in the North Atlantic is of significantly different character from those for rays bottoming under Western Russia and southeast and central Europe (for details, see Figs. VI.4.1, VI.4.2 and VI.4.3). The differences arise principally from variations in the outer 2-300 km of the three regions and from the apparently anomalous nature of the velocity distribution between 300 and 500 km beneath southern and central Europe. Extremal 'Tau'-inversion is extended to the calculation of bounds on vertical transit time for different depth ranges beneath the three regions. A maximum difference of 3 s is permitted in the two-way vertical transit times of P waves between 50 and 800 km below western Russia and the North Atlantic. The bounds obtained on transit times between 300 and 800 km demand no difference between the two regions and permit a maximum difference of 1.5 s in two-way transit time. This is consistent with the observation

that the North Atlantic travel time curve may be fitted to within error by a model which is substantially the same as that for western Russia below 300 km.

P.C. England,^{*} Univ. of Cambridge
B.L.N. Kennett, Univ. of Cambridge
M. Worthington, Univ. of Oxford

^{*} Formerly NTNF/NORSAR

References

- Bessonova, E.N., V.M. Fishman, V.Z. Ryaboyi and G.A. Sitnikova (1974):
The tau method for the inversion of travel times: Deep seismic
sounding data, Geophys. J.R. Astr. Soc., 36, 377.
- England, P.C., B.L.N. Kennett and M.H. Worthington (1977): A comparison
of the upper mantle structure beneath Eurasia and the North Atlantic,
submitted for publication.
- England, P.C., M.H. Worthington and D.W. King (1977): Lateral variations
in the structure of the upper mantle beneath Eurasia, Geophys. J.R.
Astr. Soc., 48, 71.
- Kennett, B.L.N. (1976): A comparison of travel time inversions, Geophys.
J.R. Astr. Soc., 44, 517.
- King, D.W., and G. Calcagnile (1976): P-wave velocities in the upper
mantle beneath Fennoscandia and Western Russia, Geophys. J.R. Astr.
Soc., 46, 407.

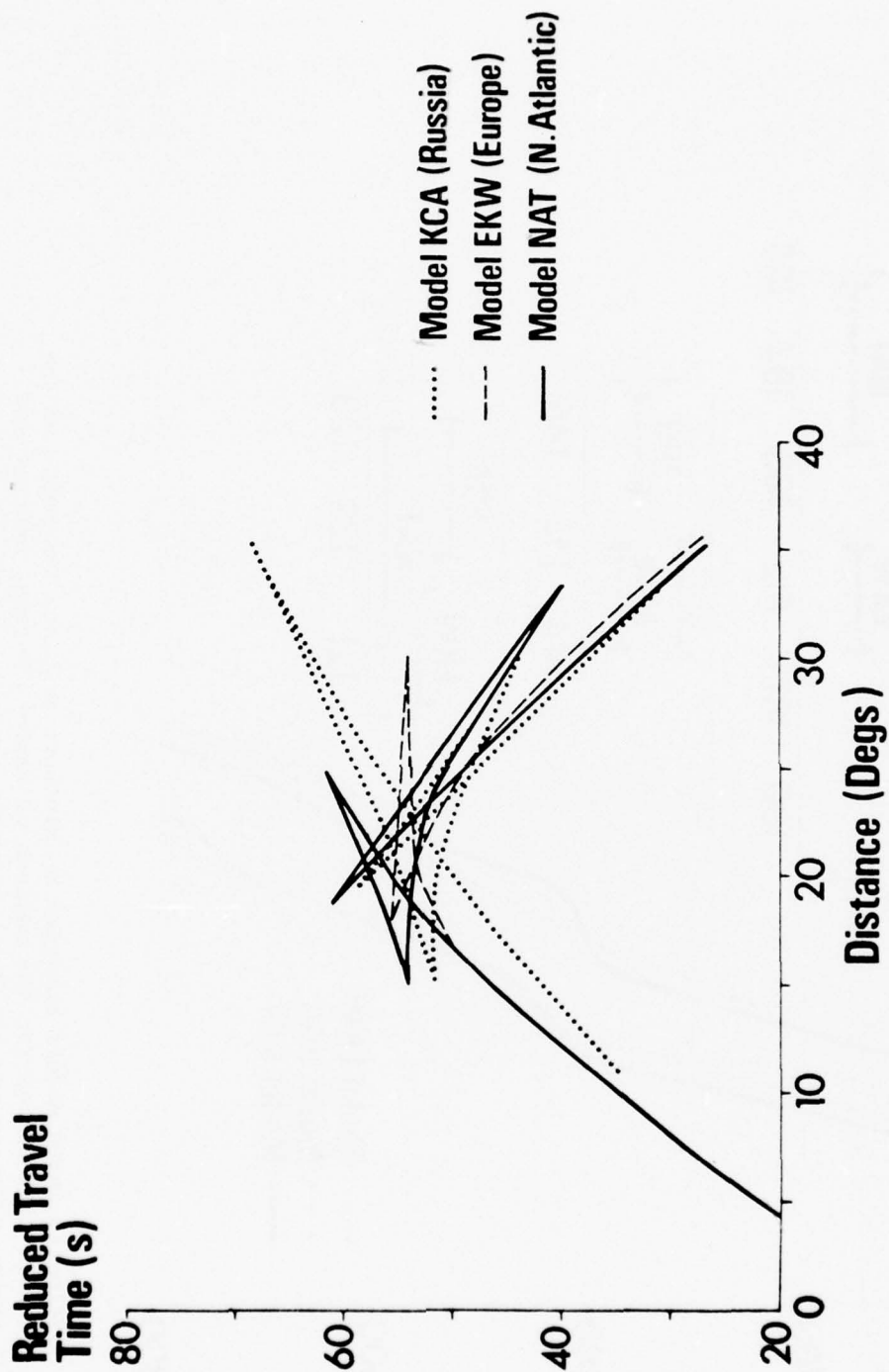


Fig. VI.4.1 Comparison of the reduced travel time curves generated from the three velocity models shown in Fig. VI.4.2. (Figure reproduced from England, Kennett and Worthington, 1977.)

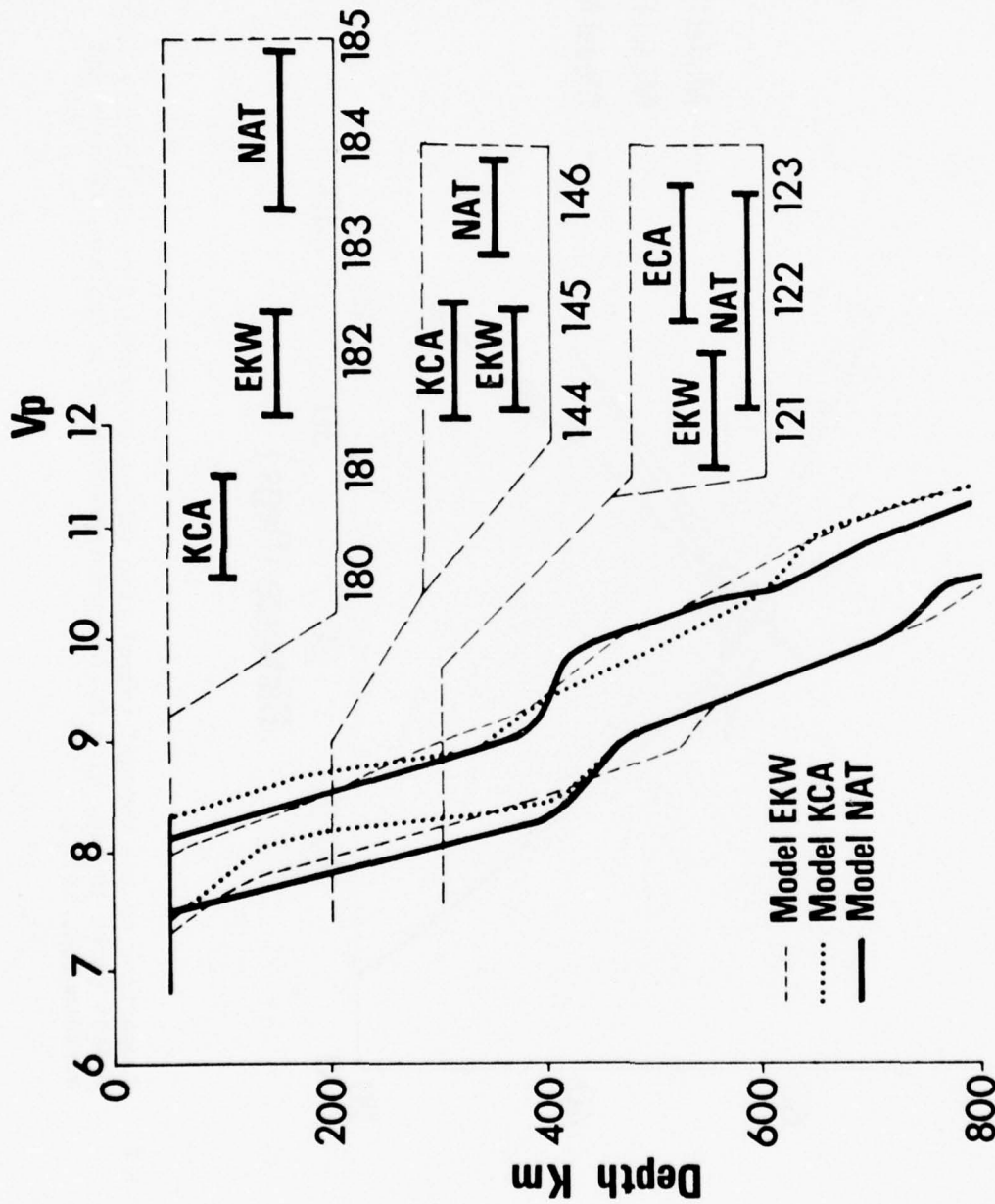


Fig. VI.4.2 Velocity depth models obtained by Wiechert-Herglotz inversion of the travel time curves for the regions of Western Russia, central and southern Europe and the North Atlantic. (Figure reproduced from England, Kennett and Worthington, 1977.)

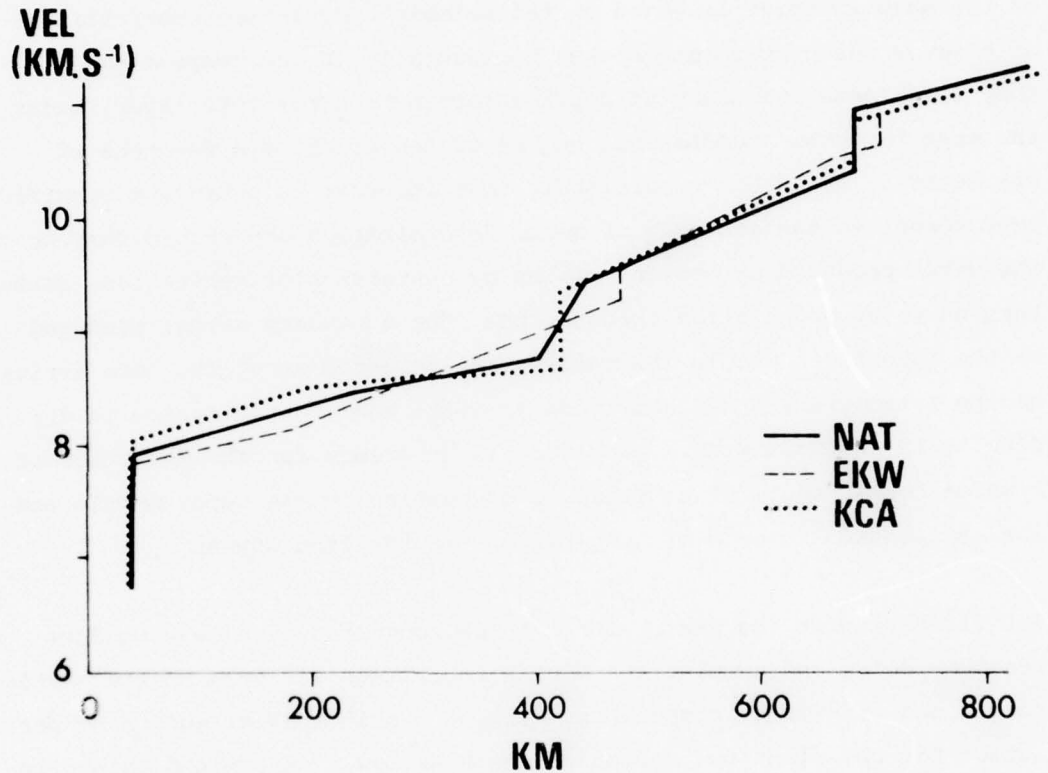


Fig. VI. 4.3 Velocity-depth bounds obtained by tau inversion of the three travel time curves represented in Fig. VI.4.1, and bounds on the two-way vertical transit times between 50 and 800 km, 200 and 800 km and 300 and 800 km for each pair of velocity-depth bounds. (Figure reproduced from England, Kennett and Worthington, 1977.)

VI.5 Detection of Waves Converted from P to SV in the Mantle

According to various seismological studies the uppermost part of the mantle includes a number of discontinuities probably produced by phase transitions. The principal method used for structural investigations of the deep interior is based on teleseismic travel-time observations of P waves which propagate almost horizontally in the deepest layer they illuminate. Accuracy of depth determination for this layer, under the most favorable conditions, may be of the order of a few tens of kilometers. The author's opinion is that in order to achieve a significant improvement in the accuracy of depth determination one should rely on the waves produced at the interfaces by conversion or reflection, rather than on waves propagating through them. The secondary waves, produced at the interfaces within the mantle, are recorded among the late arrivals of the seismogram; their amplitude is small and identification is difficult. In the following a procedure is described for the detection of P waves converted to SV at presumed boundaries in the upper mantle and its application to sets of long-period records from NORSAR

The first step in the search for P to SV converted waves was to form beams by delay and summing the NORSAR recordings for each of the vertical, radial and transverse components. Next, the principal direction of particle motion for the first few cycles of the P wave was determined using the method of Husebye et al (1975). Then the particle motion was projected on an axis which lies in the vertical plane containing the principal direction and at the same time is perpendicular to the same direction. Such projection is optimum for detection of SV while at the same time it is suppressing P-wave motion.

In order to form a basis for comparison between the converted phases which may be present in the codas from events with different signal shapes, the records were converted to a similar form by convolving the component $H(t)$ for each event with the corresponding component of the P wave and normalized with respect to the energy of this component. The record formed by this convolution process is demonstrated in Fig. VI.5.1.

The possibility of detecting weak converted phases is further enhanced by stacking: i.e., the summation of $\hat{A}(t)$ for many events with appropriate time delays is demonstrated in Fig. VI.5.2. The figure shows three distinct phases with their maxima occurring at different sets of delays. The first, with a maximum at about 15 s after the P onset, decreases as the phasing depth is increased. This phase may be associated with crustal SV conversion. The second and third peaks albeit small correspond to depths around 420 and 670 km.

The interpretation of the phases found around 45 and 70 s as conversions from P to SV at boundaries in the 410-440 km and 640-690 km depth ranges is supported by the fact that the times coincide almost exactly in two different frequency bands. Most important, however, is the fact that the maximum amplitudes of the identified converted phases on the stacked beams coincide in time and stacking velocity. That is, the phase at a delay time of around 45 s has its maximum amplitude for the stacked beams steered towards 420 km, which is the proper depth for such a delay time. Similarly the phase at a delay time of around 70 s has its maximum amplitude for stacked beams steered towards 660-680 km depths, which again is the correct depth.

Finally, an advantage of the approach described here is that the estimates of depth apply to the vicinity of the receiver. Moreover, the method can be applied to records of a single three-component long-period set. For further details, see Vinnik (1977).

L.P. Vinnik, Inst. of Physics
of the Earth, Moscow

(Formerly NTNF/NORSAR Visiting
Scientist)

Reference

- Vinnik, L.P. (1977): Detection of waves converted from P to SV in the mantle, *Phys. of Earth and Planet. Inter.*, 15, 39-45.

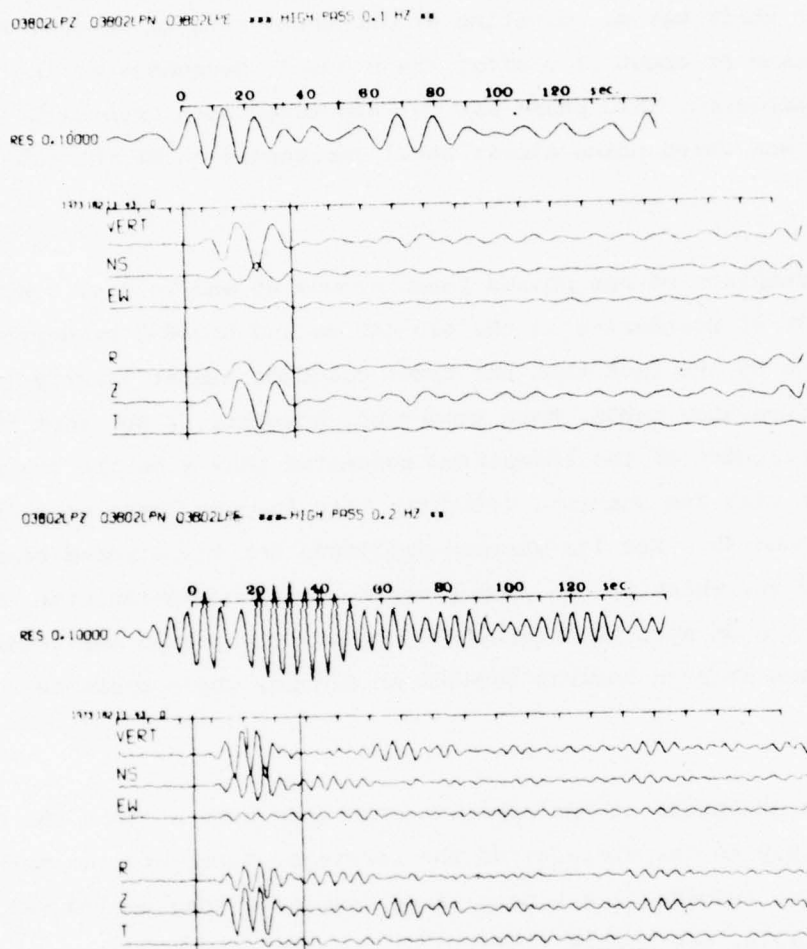


Fig. VI.5.1 The filtered records from the long-period instrument subarray 4 for an earthquake in Alaska, 1 July 1973. The upper set of traces shows the signal subjected to a high-pass filter with a cut-off frequency of 0.1 Hz; the vertical, NS- and EW-components are shown, as well as the rotated radial (R) and transversal (T) components. The vertical lines mark the interval of P used in forming the convolved record $\hat{A}(t)$ shown immediately above these records. The lower set of traces corresponds exactly to the upper except that the cut-off frequency is here 0.2 Hz.

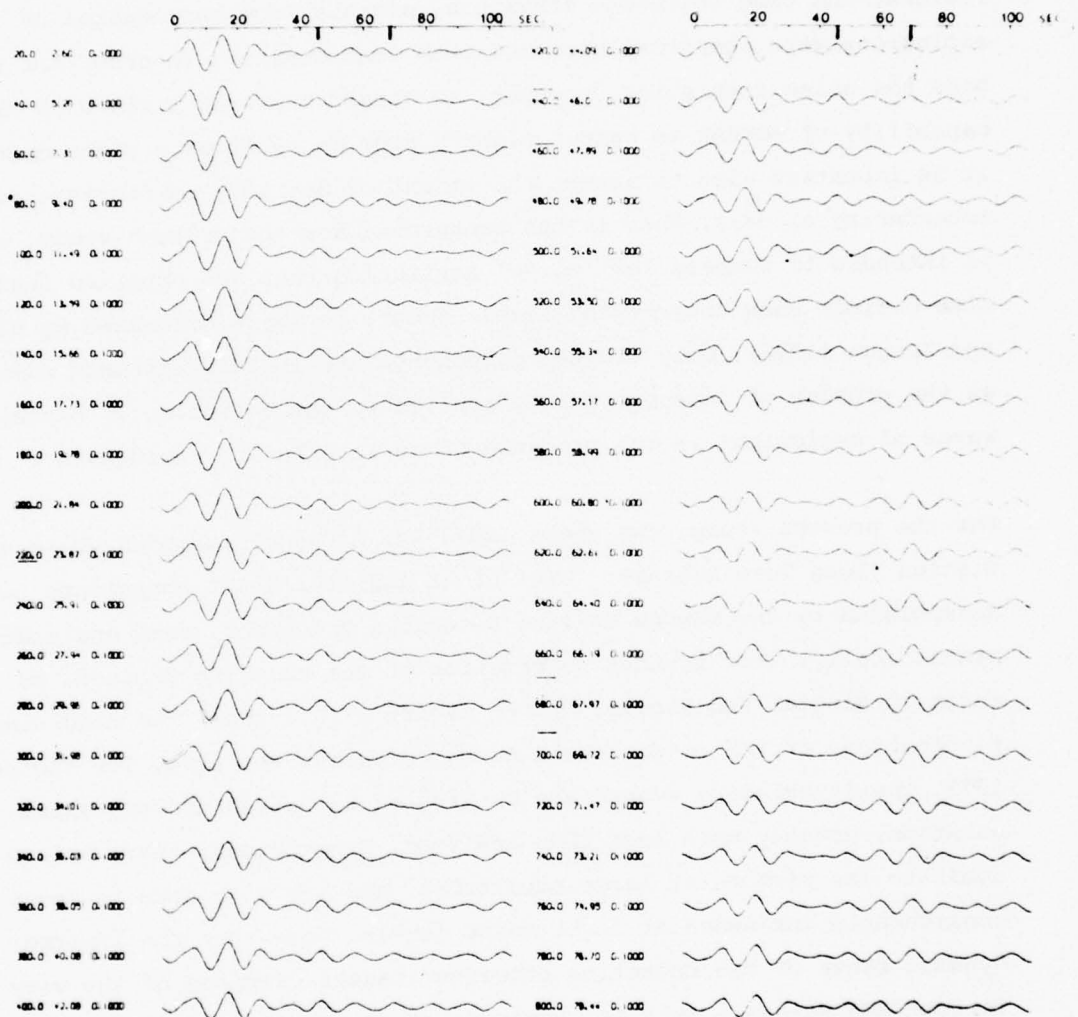


Fig. VI.5.2

Beams formed from the records of 22 earthquakes with time delays corresponding to depths from 20 to 800 km in steps of 20 km. The phasing depths are shown in the first column, the second column shows the theoretical arrival time after P for an SV wave arising from a conversion at the phasing depth. The marks on the time axis are at 45.5 and 68.5 s.

VI.6 Long Period Noise Level Variations at NORSAR

Ringdal and Bungum (1977) have in a comprehensive study discussed the effect of noise level variations on the NORSAR detectability of seismic events. The paper was confined to the study of microseismic noise conditions, and time intervals containing signals from earthquakes or explosions were therefore excluded from consideration in order not to bias the noise statistics. However, to obtain a proper picture of the capability of NORSAR to detect signals from an event of a given magnitude, it is important also to assess the amount of degraded performance due to interfering signals. This is the background for the present study, which is intended to compare the 'noise' statistics that are obtained including time periods when interfering events occur, to those discussed by Ringdal and Bungum (1976). Only the LPZ components are included in this summary, as the problem of interest mainly applies to the detection of Rayleigh waves of explosions in the presence of an interfering earthquake.

For the present study, two years (1973-74) of hourly sampled noise statistics (Long Term Average - LTA) of 22 unfiltered LPZ components, as accumulated by the NORSAR On-line Detection Processor, were analyzed statistically. (For further description of the sampling process, we refer to Ringdal and Bungum, 1977.) Figure VI.6.1 shows the resulting fluctuations of RMS noise levels averaged across the array for the year 1973. The interfering events are manifested as spikes of very short duration, usually much less than one hour. Nonetheless, these spikes dominate the picture at large amplitudes, and are also seen to cause considerable influence at lower noise levels. Note that the limited dynamic range of the detection processor causes clipping of the very largest RMS values - this is, however, of no consequence in the following discussion.

Figure VI.6.2 shows cumulative noise level statistics over the two years 1973-74. The plots are made on normal probability paper, with logarithmic scaling of the amplitude axis. We note that each of the two distributions appears slightly curved, and thus may not be well approximated by a straight line over the whole range of values. This indicates that the commonly assumed lognormal distribution of noise amplitudes at a given station may not be entirely adequate for long period data. Comparing the

two distributions, we note that the influence of including time intervals of interfering events in the observations is of little consequence at the 50 per cent level (a difference of only 1.4 dB or less than 0.1 M_s units). Even at the 90 per cent level the difference is modest (3.2 dB). However, at higher probability levels the two distributions diverge rapidly, and their difference reaches 12 dB at 99 per cent level. It is expected that the differences at low probability levels would be more significant in a narrow frequency band around 20 seconds period than in the wide-band case considered here, since small signals would then more easily influence the noise level. Thus, von Seggern and Blandford (1976) obtained differences of nearly 0.3 magnitude units at the 50 per cent level when considering noise peaks of periods around 20 seconds observed at the VLPE station at Charters Towers, Australia. One should, however, remember that the expected decrease in detectability in the presence of interfering events could be partly offset by applying multichannel techniques to suppress the unwanted signals.

In conclusion, in a statistical model, it appears that the presence of interfering events will have a relatively modest influence on the NORSAR detection probability of surface waves, up to the 90 per cent level. Above this level, the influence will be more significant, and should be dealt with accordingly when establishing models either for NORSAR detection capabilities or for the surface wave detection capability of global networks.

F. Ringdal

References

- Ringdal, F., and H. Bungum (1977): Noise level variation at NORSAR and its effect on detectability, *Bull. Seism. Soc. Amer.*, 67, 479-492.
- von Seggern, D., and R. Blandford (1976): Seismic threshold determination, *Bull. Seism. Soc. Amer.*, 66, 753-788.

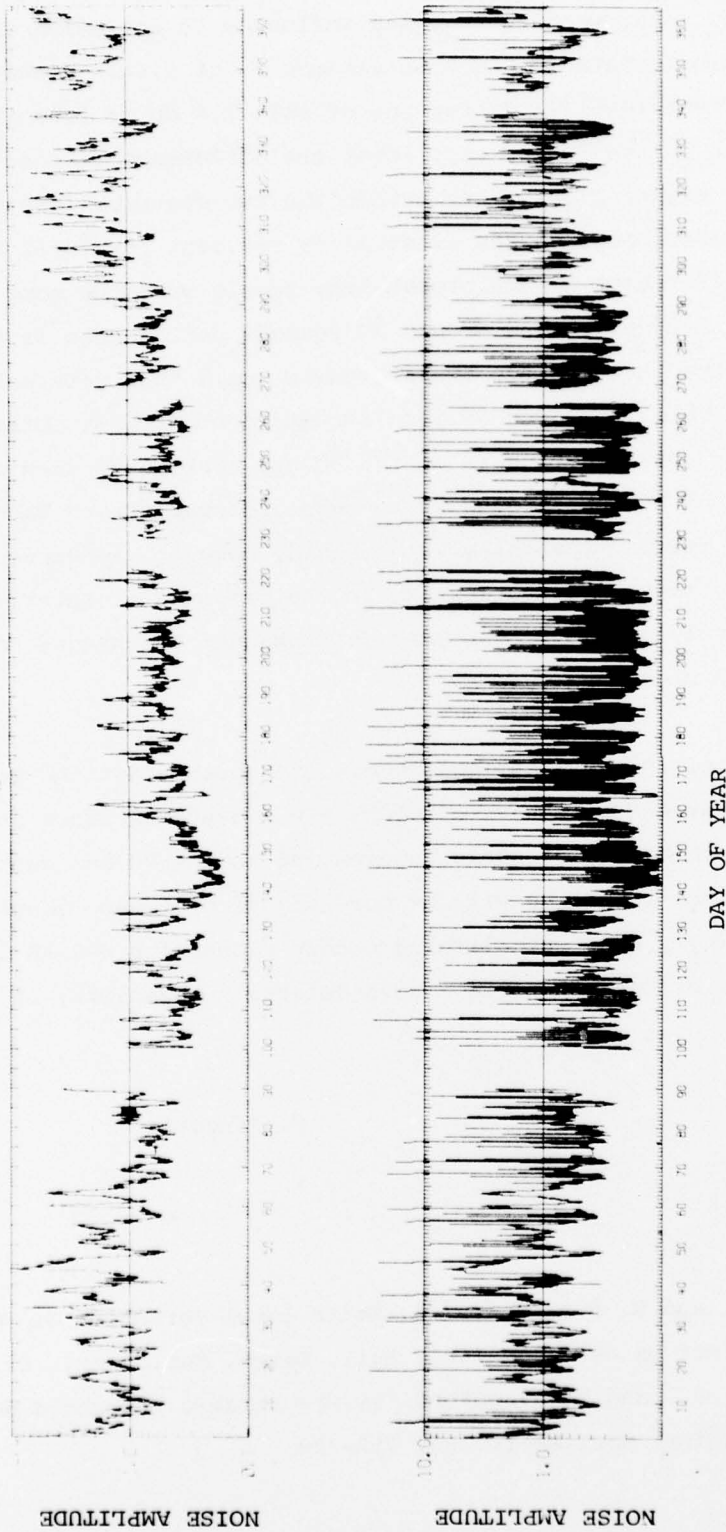


Fig. VI.6.1 Fluctuations in seismic noise level at NORSAR (average RMS value across the array for LPZ instruments) during the year 1973. The upper curve represents data where time intervals containing signals from interfering events have been excluded from consideration. The lower curve has been obtained not applying these restrictions, i.e., using the entire time interval. Both curves are scaled relative to the average value during the year.

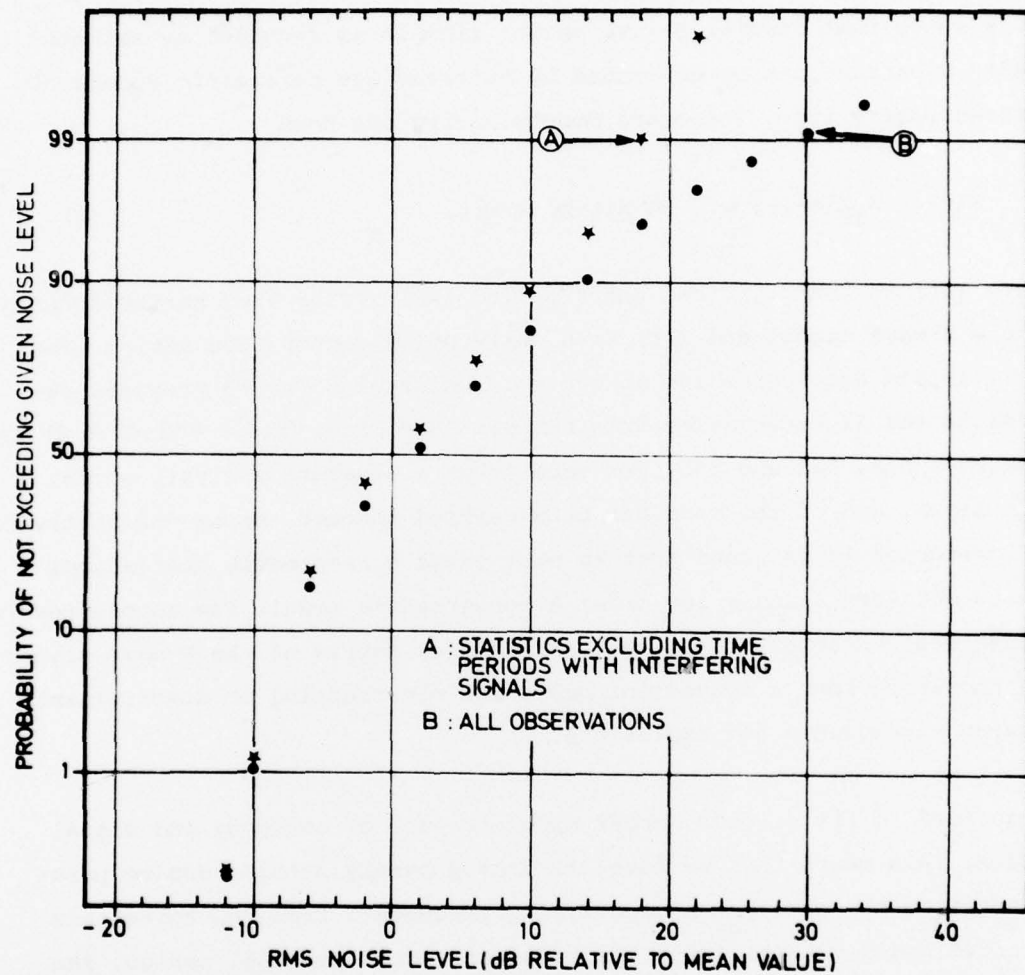


Fig. VI.6.2

Cumulative RMS noise level statistics for the average LPZ channel (unfiltered) at NORSAR during the years 1973-74. Two cases are displayed, one including and one excluding time periods where interfering signals from earthquakes have occurred.

VI.7 Short-period Discrimination Using Multivariate Autoregressive Representation of P-waves

It is shown that seismic P-wave vector signals as recorded by selected NORSAR subarrays can be described by multivariate parametric models of autoregressive type. These are models having the form

$$\underline{X}(t) - A_1 \underline{X}(t-1) - \dots - A_p \underline{X}(t-p) = \underline{W}(t) \quad (1)$$

where $\underline{X}(t)$ is the digitized short-period (SP) vector time series defined by the P-wave signal and $\underline{W}(t)$ is a white noise vector time series. The multivariate autoregressive analysis is undertaken for 83 presumed explosions and 72 earthquakes from Eurasia (see Figs. VI.7.1 and VI.7.2) using subarrays 01A, 02C and 04C. For each event a separate analysis of the main signal and of the coda has been carried through. Using the multivariate FPE criterion it is found that in most cases a reasonable statistical fit is obtained using a low order autoregressive model. The autoregressive parameters characterize the spectral density matrix of the P-wave signal and therefore form a convenient basis for constructing SP discriminants between earthquakes and explosions.

We decided to fit a second order model to each of the coda and signal series. This means that we have $2 \cdot 2 \cdot 3 \cdot 3 = 36$ purely autoregressive parameters from the matrices A_i and $2 \cdot 6 = 12$ parameters from the covariance matrices $K = E\{\underline{W}(t) \underline{W}(t)^T\}$ for the coda and signal residual series. The parameters of the K-matrices were replaced by one SP scaling parameter, namely, m_b . Thus we end up with a primary feature vector \underline{Y} of dimension 37. This parameter vector was subsequently reduced to a 9-dimensional secondary feature vector using principal component analysis. Finally we used the classifier $S_1(\underline{Z}) - S_2(\underline{Z})$ given in formula (3) of Tjøstheim (1977).

For matters of comparison we treated the $m_b : M_s$ data and the $a_{31} : a_{32}$ discriminant of Tjøstheim (1975) in a similar way. From Fig. VI.7.3 it is seen that the new multivariate autoregressive discriminant has a substantially larger discrimination potential than the parameters a_{31}, a_{32} .

The $a_{31}:a_{32}$ discriminant on the other hand is thought to be fairly representative for most SP discriminants proposed in the literature; compare Dahlman and Israelson (1977, p. 248). Moreover, a comparison with the $m_b:M_s$ data on Fig. VI.7.3 indicates that it may now be possible to construct purely SP discriminants which are comparable, if not superior, to the $m_b:M_s$ criterion.

O.A. Sandvin and D. Tjøstheim

References

- Dahlman, O., and H. Israelson (1977): Monitoring Underground Nuclear Explosions, Elsevier, Amsterdam.
- Tjøstheim, D. (1975): Autoregressive representation of seismic P-wave signals with an application to the problem of short-period discriminants, Geophys. J. R. Astr. Soc., 43, 269-291.
- Tjøstheim, D. (1977): A pattern recognition approach to seismic discrimination. Part II: Classification, Semiannual Technical Summary, NORSAR Sci. Rep. No. 2-76/77, 61-63.

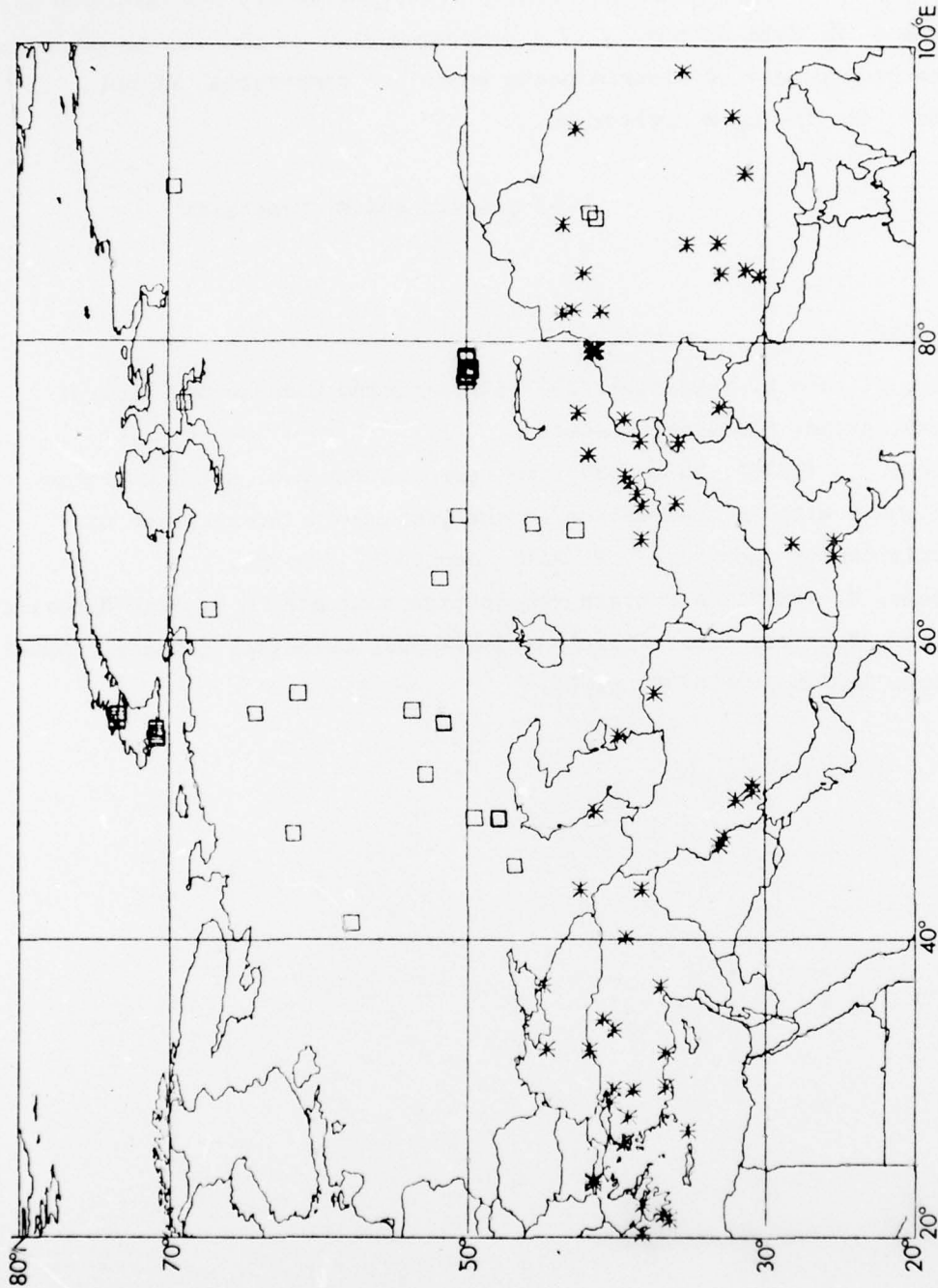


Fig. VI.7.1 The geographic distribution for the data set of 83 explosions and 72 earthquakes. Explosions are depicted by squares and earthquakes by stars in this figure as well as in figures VI.7.2 and VI.7.3.

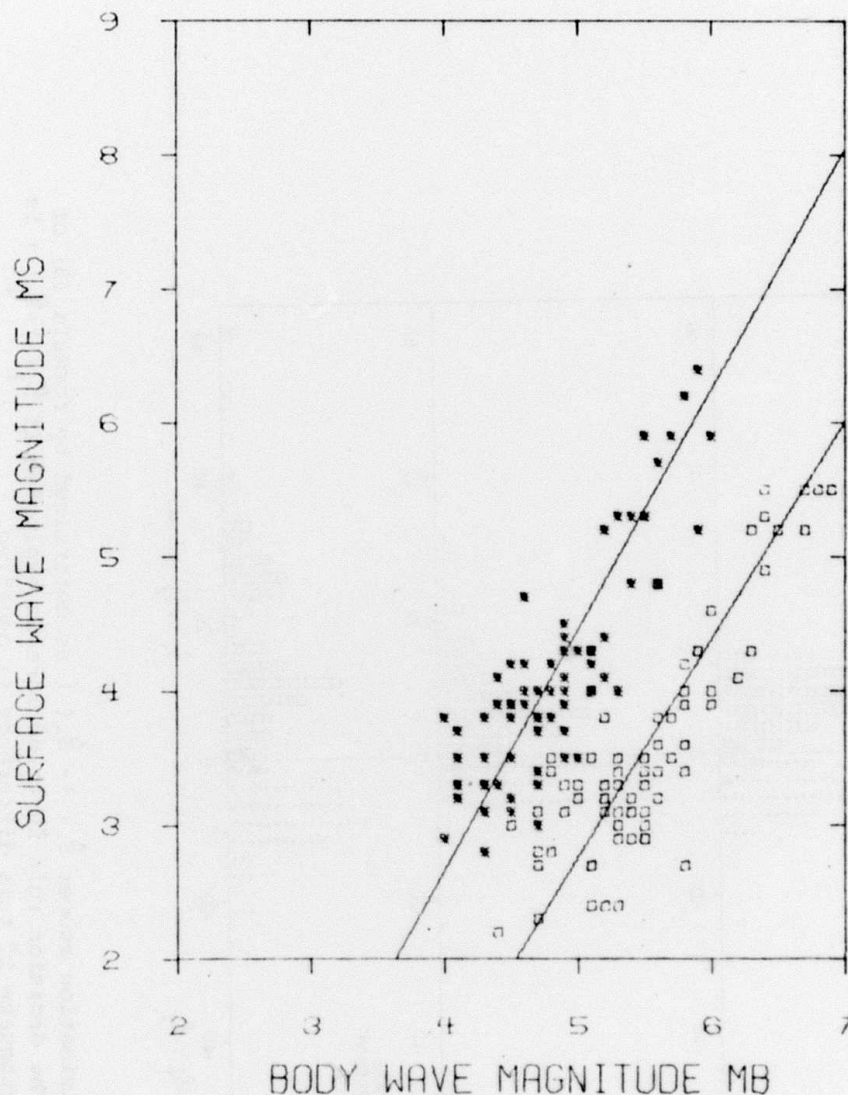


Fig. VI.7.2 $m_b:M_s$ diagram for the data set of 83 explosions and 72 earthquakes. PDE m_b and NORSAR M_s values have been used. Vertical component Rayleigh waves were not detected for 20 of the explosions. These events have been provided with an upper limit for a surface wave magnitude M_s by measuring the amplitude of the largest noise cycle within a time window of about 1 minute covering the expected arrival time of the 20 s Rayleigh wave component.

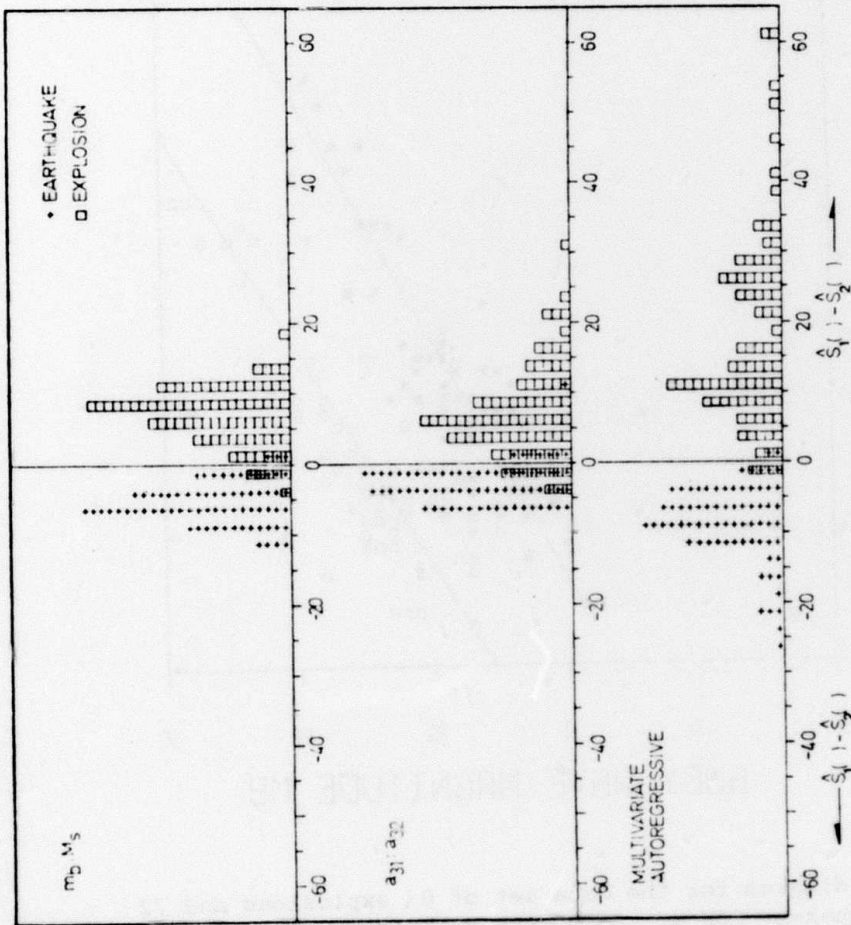


Fig. VI.7.3 Histogram of discrimination scores $\hat{S}_1(\cdot) - \hat{S}_2(\cdot)$ as determined by formula (3) of Tjøstheim (1977). The decision rule is to declare an explosion if $\hat{S}_1(\cdot) - \hat{S}_2(\cdot)$ is positive and an earthquake if this difference is negative.

VI.8 A Measure of Association for Spatial Variables

Motivated by problems in a statistical modelling of air pollution data, we propose a measure of association for two spatial variables $F(\underline{x})$ and $G(\underline{x})$. The new measure supplements the conventional correlation and rank correlation coefficients. Because of its general nature, the measure is applicable also to spatial geophysical data and in particular to seismological array data.

The measure is based on the ranks of the observations and on the location coordinates of the measurement points: If spatial location coordinates for large F -values correspond closely to spatial locations for large G -values and similarly for small values, the two variables will be assigned a high positive degree of association. High negative degree of association is assigned if spatial locations of large values for one variable correspond to spatial locations of small values for the other variable and vice versa. For independent spatial variables $F(\underline{x})$ and $G(\underline{x})$ it is shown that under optimal coordinate designs the variance of the measure is of order $1/kn$ where n is the number of data points and $k = \dim \underline{x}$ is the dimension of the observation space. Conditions for asymptotic normality are developed, and asymptotic formulae for bias and variance are found also in the case of sampling from a population with a finite number of measurement points.

D. Tjøstheim

Reference

Tjøstheim, D. (1977): A measure of association for spatial variables, *Biometrika*, in press.

VI.9 A Criterion for Determining the Order of an AR Model

In geophysical time series modelling the observed time series are often sought approximated by autoregressive (AR) time series. This is for example the case in maximum entropy spectral estimation. The most used criterion for determining the order p of an autoregressive model

$$X(t) - a_1 X(t-1) - \dots - a_p X(t-p) = Z(t) \quad (1)$$

is the Akaike FPE criterion given as

$$\hat{FPE}(p) = \frac{N+p}{N-p} \hat{\sigma}_Z^2(p) \quad (2)$$

where $\hat{\sigma}_Z^2 = \frac{1}{N} \sum_{t=1}^N |Z(t)|^2$ is the estimated residual variance and N is the number of observations of $X(t)$. The FPE criterion picks the order p for which $\hat{FPE}(p)$ takes its minimum. Based on a paper by Schwarz (1976) we suggest a new criterion, the AMBE (Asymptotic Maximum Bayes Estimator) which is defined as

$$\hat{AMBE}(p) = N \log \hat{\sigma}_Z^2(p) + p \log N \quad (3)$$

The integer p corresponding to the minimum value of $\hat{AMBE}(p)$ is adopted as the order of the time series. The two criteria were compared in a number of simulation experiments. For the series given in Table VI.9.1 it is seen that the AMBE criterion performs considerably better than the FPE criterion. Further experiments are presently being conducted for higher order models. The preliminary results obtained suggest that the performance of the two criteria are approximately the same here.

O.A. Sandvin and D. Tjøstheim

References

- Sandvin, O.A. (1977): Modelling and Application of Parametric Time Series, Cand. real. thesis, University of Bergen, Norway.
- Schwarz, G. (1976): Estimating the dimension of a model. The Inst. of Advanced Studies, The Hebrew University of Jerusalem.

Table VI.9.1

20 realizations have been generated for each AR model. The mean value, standard deviation as well as the maximum and minimum value of the orders picked by the AMBE and FPE criteria, respectively, have been tabulated for each model.

Order	Simulated AR-models						Mean Value of AMBE	Standard Deviation of AMBE	Mean Value of FPE	Standard Deviation of FPE	Max-Min Order from AMBE	Max-Min Order from FPE
	a_1	a_2	a_3	a_4	a_5	σ_z^2						
2	1.60	-0.63	-	-	-	5.00	2.00	0.00	2.60	0.75	2 - 2	4 - 2
2	1.75	-0.72	-	-	-	10.00	2.25	0.42	2.80	0.67	3 - 2	4 - 2
2	0.30	0.60	-	-	-	5.00	2.15	0.39	2.90	1.35	3 - 2	7 - 2
3	0.80	0.82	-0.64	-	-	5.00	3.00	0.00	3.40	0.65	3 - 3	6 - 3
4	-0.30	1.05	0.18	-0.25	-	10.00	4.00	0.00	4.50	1.02	4 - 4	7 - 4
4	0.20	-1.16	-0.18	0.30	-	10.00	4.15	0.35	4.45	0.74	5 - 4	6 - 4
5	0.71	1.44	-0.80	-0.30	0.21	5.00	4.80	0.60	5.40	1.35	5 - 3	8 - 3
5	0.36	1.30	-0.54	-0.40	0.18	10.00	4.85	0.40	5.50	1.05	5 - 4	8 - 4

VI.10 A New Method of Spectral Estimation for Spatial Data. Part II

We have continued the experiments described in Tjøstheim (1977). In particular we have tried to implement a spatial version of the AMBE criterion given in Eq. (3) of Sandvin and Tjøstheim (1977). For a geophysical quantity $F(x) = F(x_1, x_2)$ defined on a regular grid in the x_1 - x_2 plane the AMBE criterion is defined as

$$\hat{AMBE}(p_1, p_2) = \left(\prod_{i=1}^2 N_i \right) \log \hat{\sigma}_z^2(p_1, p_2) + \left(\prod_{i=1}^2 (p_i+1)-1 \right) \log \prod_{i=1}^2 N_i \quad (1)$$

where p_i is the order and N_i the number of observations in the x_i -direction $i=1,2$, and where $\hat{\sigma}_z^2(p_1, p_2) = E|Z(x_1, x_2)|^2$ is the residual variance for an $AR(p_1, p_2)$ model. The pair of integers (p_1, p_2) for which $AMBE(p_1, p_2)$ takes its minimum is adopted as the order of the AR model. As in Sandvin and Tjøstheim (1977) we did a number of experiments on artificially generated models. The results of Table VI.10.1 again suggest the superiority of the AMBE criterion for 'ordinary' autoregressive models in the plane. The effect on spectral estimation is illustrated in Fig. VI.10.1 for model 3 of Table VI.10.1. It is seen that the overestimation of order brought about by the FPE criterion leads to a quite severe distortion of the spectrum. It should be noted also that the autoregressive AMBE spectrum (Fig. VI.10.1b) gives a much more accurate picture of the true spectrum than the FFT spectrum (Fig. VI.10.1d).

Unfortunately the AMBE criterion does not work very well on singular models of type

$$F(x_1, x_2) = Z(x_1, x_2) + A \cos(\alpha_1 x_1 + \alpha_2 x_2) + B \cos(\beta_1 x_1 + \beta_2 x_2) \quad (2)$$

where we have two cosines embedded in two-dimensional spatial white noise. Especially for weak harmonic signals (small values of A and B) the low reduction in variance at each step of the autoregressive approximation implies that the last term in (1) dominates the first one for moderate values of (p_1, p_2) and there is a tendency for the AMBE criterion to predict models on the 'edge', i.e., degenerate models

of type $(0, p_2)$ or $(p_1, 0)$. The spatial FPE criterion performs somewhat better in this respect.

D. Tjøstheim

References

Sandvin, O.A., and D. Tjøstheim (1977): A criterion for determining the order of an AR model. This report.

Tjøstheim, D. (1977): A new method of spectral estimation for spatial data. Semiannual Technical Summary, NORSAR Sci. Rep. No. 2-76/77, 64-66.

Table VI.10.1

Estimated orders (p_1, p_2) as obtained from the minimum values of the spatial FPE and AMBE criteria, respectively. The correct orders are given in the uppermost line.

Model	1	2	3	4	5
Correct Order	(1,1)	(1,1)	(1,2)	(1,2)	(3,2)
FPE	(5,1)	(4,3)	(5,2)	(5,2)	(5,2)
AMBE	(1,1)	(1,2)	(1,2)	(5,2)	(3,2)

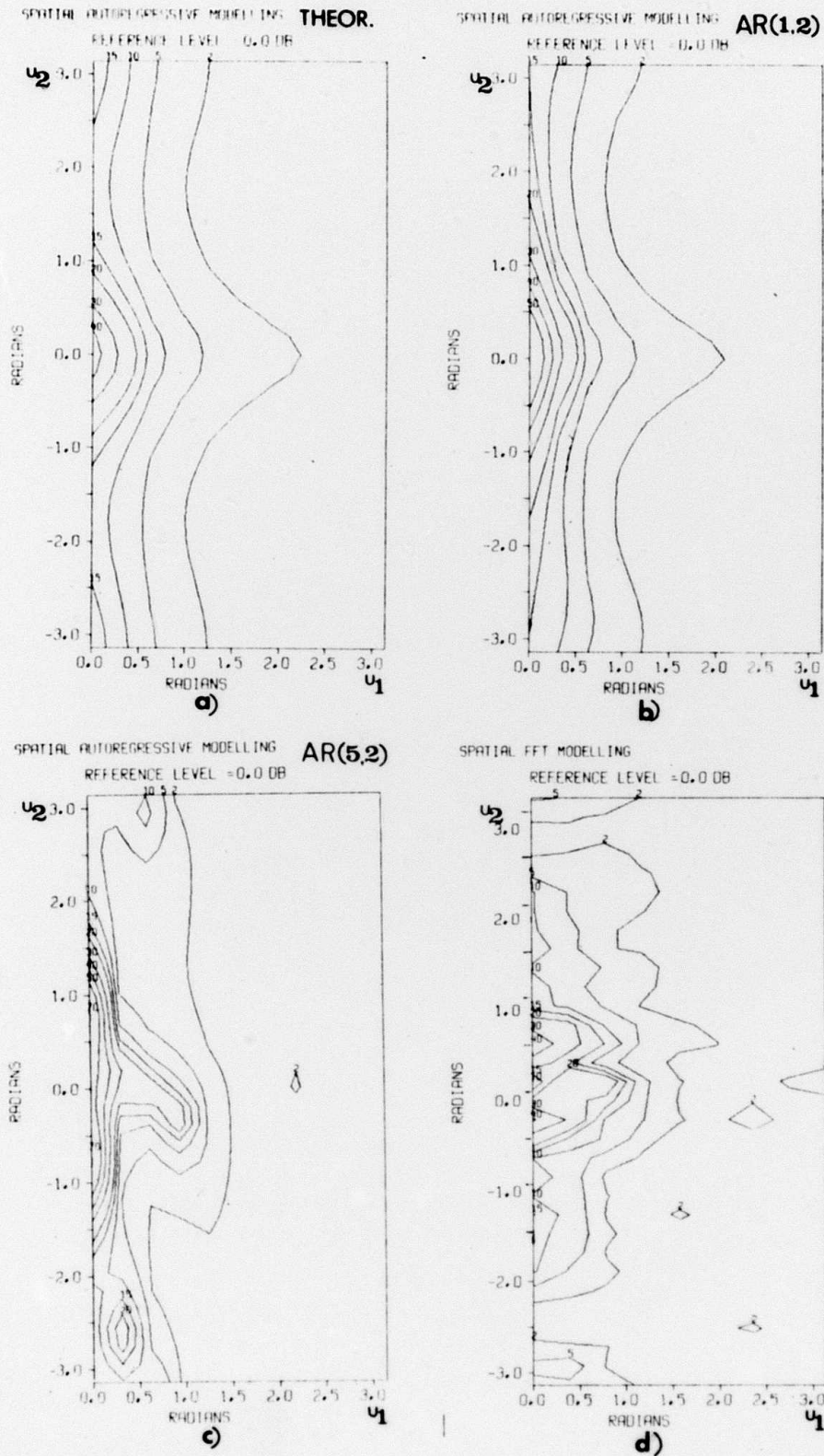


Fig. VI.10.1 a) Theoretical AR(1,2) spectrum, b) estimated AR(1,2) spectrum using the AMBE criterion, c) estimated AR(5,2) spectrum using the FPE criterion and d) estimated FFT spectrum for model 3 of Table VI.10.1 Model 3 is given as

$$F(x_1, x_2) - 0.67F(x_1 - 1, x_2) - 0.17F(x_1, x_2 - 1) + 0.11F(x_1 - 1, x_2 - 1) - 0.17F(x_1, x_2 - 2) + 0.11F(x_1 - 1, x_2 - 2) = Z(x_1, x_2).$$